

Numerical modelling of fine sediment and zinc transport in the Derwent Estuary

Derwent Estuary Program

Final Report

N. Margvelashvili, M. Herzfeld, J. Parslow



CSIRO
MARINE RESEARCH

Date: 21/12/2005

Contents

INTRODUCTION	3
MODEL	4
Hydrodynamics	4
Sediment transport	4
Metals	6
Numerical grid, initial and boundary conditions	8
CALIBRATION OF SEDIMENT MODEL	10
ADCP data	10
Sediment model vs data	14
MODELLING RESULTS	16
Sediments	16
Zinc	27
Preliminary scenario runs	31
Box-model solutions and implication for management scenarios	34
Scenarios with varying zinc loads from ground water	40
CONCLUSION	46
REFERENCES	49
APPENDIX 1: Box-model solution	51

INTRODUCTION

The Derwent estuary, in 1970-1990, was ranked as one of the most polluted estuaries in the world with respect to heavy metals (Plaschke, et al., 1997). During recent years, reduced levels of pollutants in industrial effluents have led to some improvement of the health of the Derwent, however a significant sedimentary pool of heavy metals still exists in the estuary (Green & Coughanowr, 2003). Any activity, which results in significant changes in physical or chemical conditions in bottom sediments, could raise concentrations of pollutants in water column well above the present level (Jones et al., 2003).

This report describes the development and application of a numerical model for fine-sediment and zinc transport in the Derwent estuary. The main objective of the model development is to support contaminant studies in the estuary, providing better understanding of the behaviour of the dissolved and sediment-attached pollutants. The report includes a brief description of the developed sediment/contaminant model, shows results of the sediment model calibration, and illustrates implementation of the pilot contaminant model for simulating zinc transport in the estuary.

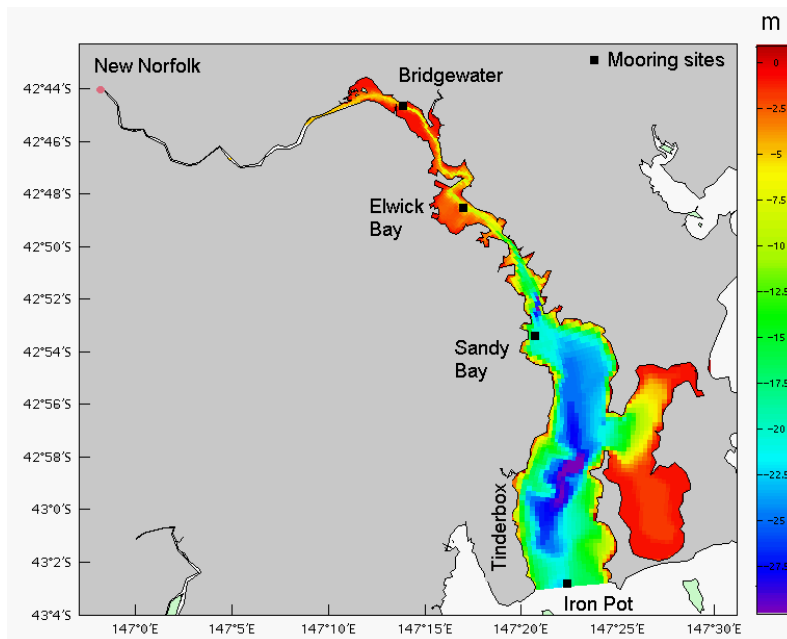


Fig 1 Bathymetry map

MODEL

Hydrodynamics

The developed sediment and contaminant models are driven by a 3-d non-linear, non-stationary, z-coordinate hydrodynamic model (Walker, 1999, Herzfeld, 2003), which solves Reynolds's equations with a free surface boundary condition, using the Boussinesq approximation and the hydrostatic assumption. The model governing equations include equations for momentum, continuity, and salinity/temperature transport. The model applications to the Derwent estuary are described in the accompanying hydrodynamic modelling report (Herzfeld et al, 2005).

Sediment transport

Mass balance equations

The sediment model solves advection-diffusion equations for the mass conservation of suspended and bottom sediments, taking into account bottom exchanges due to resuspension and deposition. The model governing equations include 3-D equations for the suspended sediment concentration (S_i),

$$\frac{\partial S_i}{\partial t} + \frac{\partial}{\partial x}(uS_i) + \frac{\partial}{\partial y}(vS_i) + \frac{\partial}{\partial z}[(w - w_{gi})S_i] = \frac{\partial}{\partial x}\left(K_h \frac{\partial S_i}{\partial x}\right) + \frac{\partial}{\partial y}\left(K_h \frac{\partial S_i}{\partial y}\right) + \frac{\partial}{\partial z}\left(K_z \frac{\partial S_i}{\partial z}\right), \quad z_{bot} < z < z_{top} \quad (1)$$

1-D equations for the bottom sediment concentration

$$\frac{\partial S_i}{\partial t} = \frac{\partial}{\partial z}\left(K_z \frac{\partial S_i}{\partial z}\right) \quad z_{deep} < z < z_{bot} \quad (2)$$

and equation for the top sediment layer coordinate (z_{bot})

$$\frac{\partial z_{bot}}{\partial t} = F_{solid} + F_{liquid}, \quad z = z_{bot} \quad (3)$$

Here F_{solid} , F_{liquid} are volumetric fluxes of solid and liquid phases through the “sediment – water” interface, respectively; S_i [kg/m^3] is concentration of the i-th fraction of the suspended or bottom sediments; K_z is diffusion coefficient associated with either turbulent mixing in water column or local bioturbation in sediment bed; K_h is horizontal diffusion coefficient in water column.

According to (1-3) the modelled sea-bed is represented by a number of vertically resolved columns with no direct horizontal exchange between adjacent numerical cells. Horizontal redistribution in the sea-bed is controlled by the sediment resuspension with the subsequent

transport in water column and deposition. Vertical transport in sediments is represented by local diffusion.

In surface water numerical grid for the sediment variables coincides with the numerical grid for the hydrodynamic model. In sediments, the model utilises time-varying, sediment thickness adapted numerical grid, with a constant thickness of the upper, active sediment layer.

Boundary conditions

At the lateral sea boundaries the model either utilizes zero-gradient boundary conditions or prescribes observed sediment concentrations. There are no fluxes of any property at the lateral solid boundaries.

Sediment fluxes at the estuarine surface ($z = z_{top}$) and at the bottom of the deepest sediment layer ($z = z_{deep}$) equal zero:

$$\left(w_{gi} - K_z \frac{\partial}{\partial z} \right) S_i = 0 \quad z = z_{top} \quad (4)$$

$$K_z \frac{\partial S_i}{\partial z} = 0 \quad z = z_{deep} \quad (5)$$

At the water – sediment interface ($z = z_{bot}$) solid fluxes are prescribed taking into account sediment resuspension and deposition:

$$\left(w_{gi} - K_z \frac{\partial}{\partial z} \right) \cdot S_i = Q_i \quad z = z_{bot} \quad (6)$$

Here Q_i [kg/(m² s)] represents either resuspension or deposition fluxes of sediment.

Fluxes and settling velocities

Volumetric solid and liquid fluxes across water – sediment interface are defined as

$$F_{solid} = \sum_{i=1}^n \frac{Q_i}{\rho_i}, \quad F_{liquid} = \sum_{i=1}^n \varepsilon_i \frac{Q_i}{\rho_i}. \quad (7)$$

Here ρ_i [kg/(m³)] is density of the sediment grains; and ε_i is the void ratio of the i-th fraction of the sediment deposits.

Resuspension and deposition of fine sediments is parameterised using Ariathurai - Krone (1976) formula:

$$Q_i = w_{g_i} S_i f_d + \left(\frac{S_i / \rho_i}{1 - \varphi} \right) M f_e, \quad (8)$$

were the probabilities for deposition and erosion are given by

$$f_d = \begin{cases} 0: & \tau_b \geq \tau_{cd} \\ \left(1 - \frac{\tau_b}{\tau_{cd}}\right): & \tau_b < \tau_{cd} \end{cases} \quad f_e = \begin{cases} 0: & \tau_b < \tau_{ce} \\ \left(\frac{\tau_b}{\tau_{ce}} - 1\right): & \tau_b \geq \tau_{ce} \end{cases} \quad (9)$$

The formulation (9) depends on the specification of bottom stress τ_b , which is calculated from the hydrodynamic model. Critical shear stresses for resuspension (τ_{ce}) and critical shear stress for deposition (τ_{cd}) are empirical constants. The resuspension rate M ($\text{kg m}^2 \text{s}^{-1}$) is specified using formulation suggested by Delo (1988) (cited in Uncles and Stephens, 1989):

$$M = 0.002 * \tau_{ce} \quad (\text{kg m}^2 \text{s}^{-1}), \quad (10)$$

The transport and fate of fine grained sediment in estuarine water is a function of the effective settling velocity of the sediment, which in turn is affected largely by flocculation effects. Following field observations and laboratory studies settling velocity of sediments during simulations varied with salinity and fine sediment concentration

$$w_{gi} = \begin{cases} w_{0i}, & \text{Salinity} < 0.1 \text{ (PSU)} \\ \max(w_{0i}, aC^b), & \text{Salinity} \geq 0.1 \text{ (PSU)} \end{cases} \quad (11)$$

where a and b are empirical constants (Dyer K.R., 1989, Wim van Leussen, 1999), and w_{0i} is settling velocity of disaggregated particles.

Metals

A large variety of modelling approaches, with different level of accuracy and complexity, has been developed over the last decades for simulating sorption reactions (Van der Lee & Windt, 2001; Honeyman & Santschi, 1988; Warren & Haack, 2001). However, a unified mathematical description of sorption on coastal sediments is still not available. Many contemporary models simulate these reactions using an equilibrium distribution coefficient (K_d) approach, which does not belong to the family of deterministic, thermodynamic models, but is still useful when no detailed information is available, or as an initial modelling attempt.

If sorption is fast relative to other environmental processes, an equilibrium distribution between the liquid and solid phases may be assumed and equilibrium sorption model can be approximated as (Ambrose et al., 1993)

$$K_{di} = \frac{\hat{C}_i^p}{\hat{C}_i^d}. \quad (12)$$

where K_{di} [m^3/kg] is an equilibrium distribution coefficient between water and I-th fraction of sediment, \hat{C}_i^p [A/kg (dry sediment)] is pollutant concentration on the I-th fraction of dry sediment, \hat{C}^d [A/m^3 (water)] is the concentration of the dissolved metal, A is a measure of the pollutant activity.

According to (12), at equilibrium the distribution of concentrations between liquid and solid phases is controlled by the distribution coefficient K_{di} . However, the total masses of dissolved and adsorbed pollutants, per unit volume of sediment-water mixture, are controlled by K_{di} and the amount of solid phase present

$$\frac{S_i}{\varphi} K_{di} = \frac{C_i^p}{C^d} \quad (13)$$

where $C_i^p = S_i \cdot \hat{C}_i^p$ [A/m^3 (mixture)] is concentration of the adsorbed metals, $C^d = \varphi \cdot \hat{C}^d$ [A/m^3 (mixture)] is the concentration of the dissolved fraction, S_i [kg/m^3 (mixture)] is the sediment concentration, and φ is porosity.

If the assumption of equilibrium distribution is not valid, then sorption dynamics can be approximated by a first order kinetic reaction (Onishi et al., 1981, 1989; Zheleznyak et al., 1992)

$$\frac{\partial C^d}{\partial t} = -a \left(\frac{S_i}{\varphi} K_{di} C^d - C_i^p \right) \quad (14)$$

$$\frac{\partial C_i^p}{\partial t} = a \left(\frac{S_i}{\varphi} K_{di} C^d - C_i^p \right) \quad (15)$$

where a is the sorption/desorption rate constant.

Time-scales of zinc sorption/desorption on/from sediments, published in scientific literature, range from minutes to months (Hatje et al., 2003, Millward & Liu, 2003, Hansen & Leckie 1998). Millward and Liu (2003) reported nonlinear desorption of Zn from estuarine sediments characterised by maximum dissolved concentration after several minutes, followed by slow readsorption onto the suspended sediment over the next hours (up to ~16 hours for readsorption in a seawater). Hatje et al (2003) studied kinetics of Zn adsorption as a function of suspended particle concentration and salinity. In concentrated suspensions (sediment concentrations exceeding ~0.1 g/L) Zn presented two-step kinetics, with a short period of relatively fast sorption (~0.5 hour) followed by a longer period (days and weeks) of redistribution to more strongly bound forms within the sediment. In suspensions with lower concentration of suspended solids (0.03 g/L) Zn sorption exhibited one-step kinetics with typical time scales ranging from days to weeks. In this study, aiming the development and preliminary application of the pilot model for Zn transport, a single rate constant is utilised to represent both sorption and desorption reactions. All scenario modelling presented in the report has been carried out assuming typical time scale of 1 day for sorption/desorption reactions. Additional simulations have been conducted using the reactions time scale of 2 days.

The distribution coefficient for zinc measured in various estuaries, as published by Turner and Millward (2002), varies from 2 to 200 m³/kg. In the Derwent estuary typical concentration of suspended solids varies from 1 to 20 g/m³, and the ratio of the particulate to dissolved zinc is typically less than 10 % (Green & Coughanowr, 2003), that gives *Kd* estimates (formula 13) ranging from 5 to 100 m³/kg, consistent with the general literature data. Most simulations, shown below, correspond to the equilibrium distribution constant *Kd*=20 m³/kg. Additional simulations have been carried out with *Kd*=100 m³/kg.

Numerical grid, initial and boundary conditions

The modelling domain extends downstream from New Norfolk along the estuary to Iron Pot. The lateral spacing of the numerical grid (fig. 2) varies from ~140 m in the upper estuary to ~ 400 m at the seaward end of the estuary. The vertical coordinate is resolved by 21 layers with 0.5m resolution in the top 8 m, and the vertical resolution gradually increases in deep water. Horizontal resolution in sediments is the same as the resolution in water column. In the vertical direction bottom sediments are resolved by two layers, with the total initial thickness of sediments of 21 cm, and thickness of the upper layer of 5 mm. The modelling period extends from May 2003 to January 2004 and includes episodic events of high fresh-water discharge (up to ~ 900 m³/s).

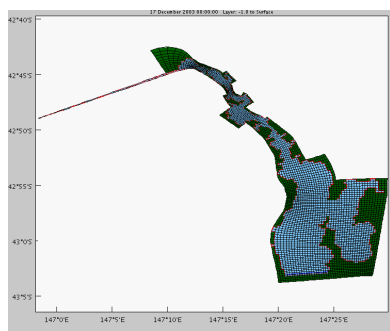


Figure 2 Plan view of the 3-D numerical grid

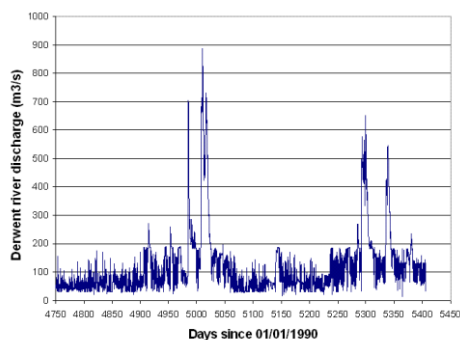


Fig. 3 Derwent river discharge

At the upstream boundary the hydrodynamic model is forced with known river flow, temperature and salinity. At the seaward boundary, temperature, salinity and surface elevation are specified by nesting inside large-scale model simulations (not shown in this report). More details on the hydrodynamic model set up and forcing are available from the accompanying report by Hertzfeld et al. (2005).

The modelled sediments are represented by sand, silt and clay fractions with the initial distribution of the bottom deposits specified from field observations (Fig. 4). Initial concentration of the suspended solids is zero. Only fine sediment transport (silt and clay) has been simulated during this study.

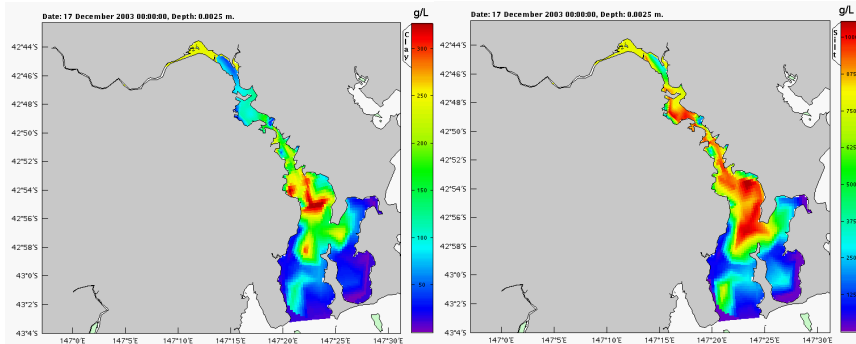


Fig. 4 Initial distributions of the clay and silt sediments in the seabed.

At the river end, constant concentrations of the suspended sediment are specified. At the seaward boundary of the model, a free-flow boundary condition is applied to all sediment fractions when the water flow is directed out of the modelling domain. During the inflow events, the sediment concentration at the seaward boundary is specified using a zero-gradient boundary condition.

One of the key parameters controlling partitioning of chemical constituents in coastal water is the composition of the sediment particles. Because of their large surface to volume ratio, fine particles can adsorb a larger amount of adsorbents than the same volume of coarser particles. Consequently, advection by fine particles is often regarded as the key transport mechanism for the sediment-bound pollutants (Ambrose et al., 1993; Onishi et al., 1981). During this study all particulate zinc was assumed to be attached to the silt and clay fractions of sediment. The measured amount of zinc per unit mass of the dry sediment has been converted to the contaminant mass per unit volume of “sediment-water” mixture, assuming a constant concentration of bottom sediments (1000 kg/m³), and then partitioned between silt and clay fractions (fig. 5).

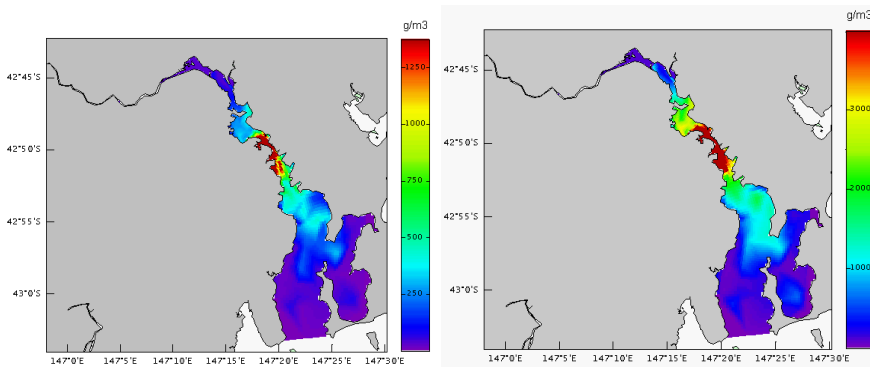


Fig. 5 Initial concentration of zinc attached to the clay and silt particles in the river-bed

CALIBRATION OF SEDIMENT MODEL

ADCP data

In order to provide better understanding of the estuarine hydrodynamics, as well as to support the sediment model developments, a relocatable ADCP has been deployed at Iron Pot, Sandy Bay, Elwick Bay and Bridgewater sites (fig. 1). The total duration of the deployments was approximately three months (from mid December 2003 to mid March 2004), with the duration of individual deployments varying from two weeks to one month.

Figure 6 shows the recorded near bottom (~ 2 m above the sea-bed) ADCP velocities and surface elevation at the deployment sites. According to the measurements, maximum velocities at Iron Pot during spring tide exceed 0.5m/s, while during the neap tide the maximum velocities are typically less than 0.2 m/s. Strong near bottom currents in excess of 0.4 m/s have also been recorded at Elwick Bay and Bridgewater sites. Sandy Bay site, located in close proximity to the coast and likely beyond the main stream of the estuarine tidal currents, is characterised by much less energetic environment with the maximum velocities of currents not exceeding 16 cm/s.

The ADCP is a robust and reliable tool for estimating flow velocity, however the application of acoustics for suspended sediment measurements is still in development. In order to calibrate the ADCP backscatter signal, suspended sediment samples have been collected from ~2 m above the sea-bed at every site during the instrument redeployment. The samples were collected using Niskin bottles, attached to the rope with a heavy weight to reduce horizontal drift of the bottle. However, because of strong currents and drifting of the boat, the sampling locations did not always coincide exactly with the locations of the ADCP. Replicate sampling conducted in Elwick Bay ~3 minutes after the first sampling indicated that an error of factor 2 is likely to be associated with the sampled sediment concentrations associated with small scale spatial and temporal variability.

The recorded ADCP voltage was related to the sampled sediment concentrations using an approach developed by Thorne et al. (1993). At a single frequency, and for a given type of sediment with a constant particle size, the suspended sediment concentrations can be expressed as (Thorne & Hanes, 1999; Holdaway et al., 1999)

$$S(r) = \left\{ \frac{V_{rms}}{K_s K_t} \right\}^2 r^2 e^{4r(\alpha_w + \alpha_s)} \quad (16)$$

where $S(r)$ is the suspended mass concentration, V_{rms} is the recorded voltage from the transducer, α_w is the attenuation coefficient due to water adsorption, and α_s is the attenuation coefficient due to scatterers in suspension. K_s contains the sediment information (scattering properties of the sediment, sediment density and mean particle radius), K_t combines a number of different aspects of the acoustic system performance (receiver sensitivity of the transducer, transceiver radius, the system gain, reference pressure at range of 1m etc.).

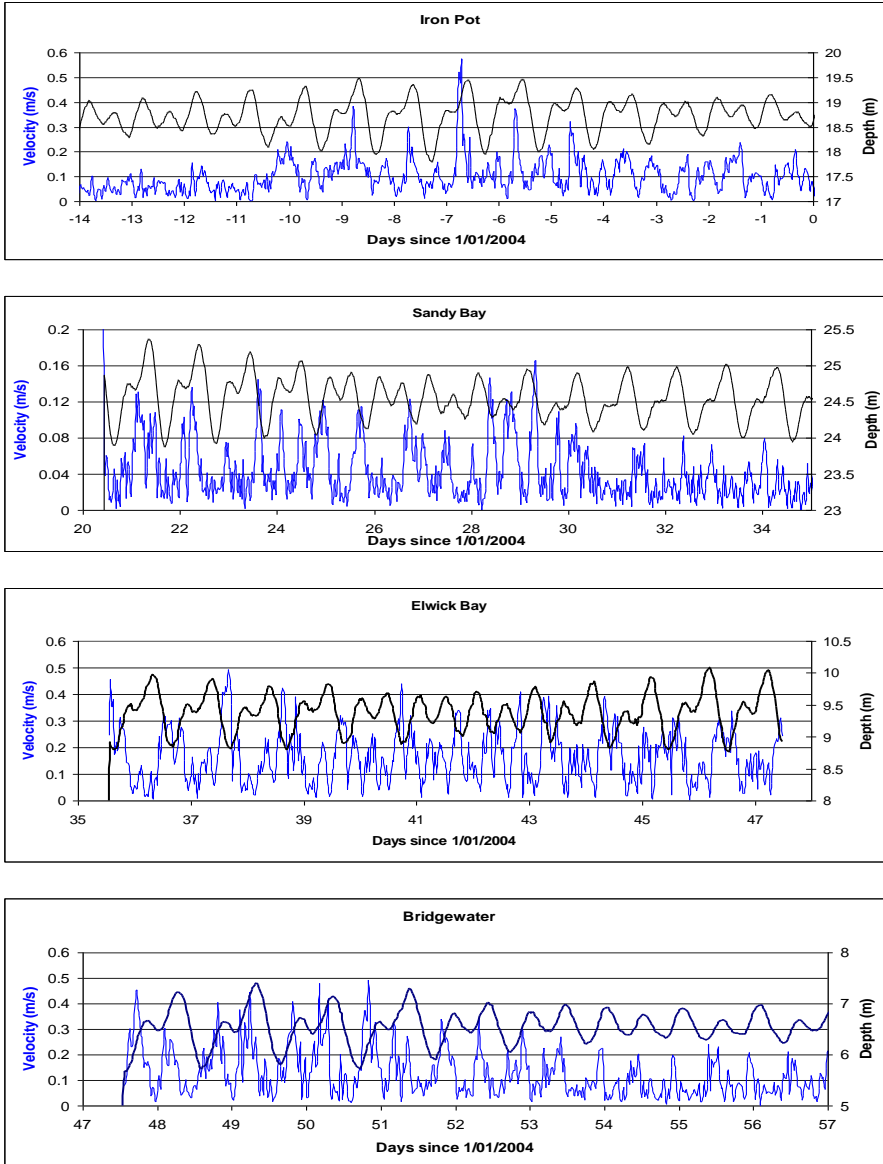


Fig 6 Measured currents and surface elevation.

The adsorption due to water α_w , required by (16), can be found from empirical formulations (Fisher et al., 1977). Attenuation due to suspended load α_s , which is associated with scattering and viscous adsorption by the suspension material, can be written as

$$\alpha_s = \frac{1}{r} \int_0^r \zeta S dr \quad (17)$$

where ζ is the sediment attenuation constant, which is a function of the acoustic signal and particle characteristics.

According to (17) evaluation of the signal attenuation due to sediments (α_s) requires a knowledge of the sediment concentration at a range from the transducer. As the sediment concentration is unknown, an iterative approach is required to solve (16). Such an approach for solving (16) has been considered by Thorne et al. (1993), who indicated that positive feedback between S and α_s can lead to the solution diverging to zero or infinity due to increasing feedback errors.

Suspended sediment concentrations observed in the Derwent estuary typically do not exceed 0.02 kg/m³ (Green and Coughanowr, 2003). Assuming a representative grain size for suspended particles of 60 μ , and using empirical formulas for the sediment attenuation from (Thorne & Hanes, 2002; formulas 8-10), the sediment attenuation constant ζ and the sediment attenuation coefficient α_s can be evaluated

$$\zeta \approx 0.004 \text{ (Nepers m}^2 \text{ kg}^{-1}\text{)} \quad (18)$$

$$\alpha_s \approx \zeta S \approx 1\text{e-}4 \text{ (Nepers m}^{-1}\text{)} \quad (19)$$

At frequencies of about 1 MHz an adsorption due to water at 14 °C, is

$$\alpha_w \approx 3\text{e-}2 \text{ (Nepers m}^{-1}\text{)} \quad (20)$$

According to (19) and (20), in the Derwent estuary, under normal conditions, the attenuation of the acoustic signal due to sediments is approximately two orders of magnitude lower than that due to water.

Assumption of the low attenuation due to sediments ($\alpha_s \ll \alpha_w$) simplifies the calibration procedure. In this case the formula (16) can be reformulated as

$$S(r) = KV_{rms}^2 r^2 e^{4r\alpha_w} \quad (21)$$

where $K = \left\{ \frac{1}{K_s K_t} \right\}^2$ is a new calibration parameter.

Figure 7 shows time-series of suspended sediment concentrations obtained from the ADCP backscatter data, using (21) and sampled sediment concentrations. According to these data, the suspended sediment concentrations at ~2 m above the seabed do not exceed 12 g/m³ at all sites. (Note that errors of at least factor 2 are likely to be associated with these estimates). Minimum concentrations of the suspended solids (less than 4 g/m³) have been recorded at Sandy Bay site, and were attributed to low velocities of the near bottom

currents. Maximum concentrations (12g/m³) were measured in Elwick Bay. The data show pronounced neap-spring variability of the suspended sediment concentrations at the Iron Pot site, and relatively strong intra-tidal variability of the suspended solids in Elwick Bay. Upon retrieval of the instrument from the Bridgewater site, the ADCP was found to be covered by a thick layer of muddy grass which likely affected the measurements and caused the rapid decline of the backscatter signal observed after 5 days from the beginning of the deployment.

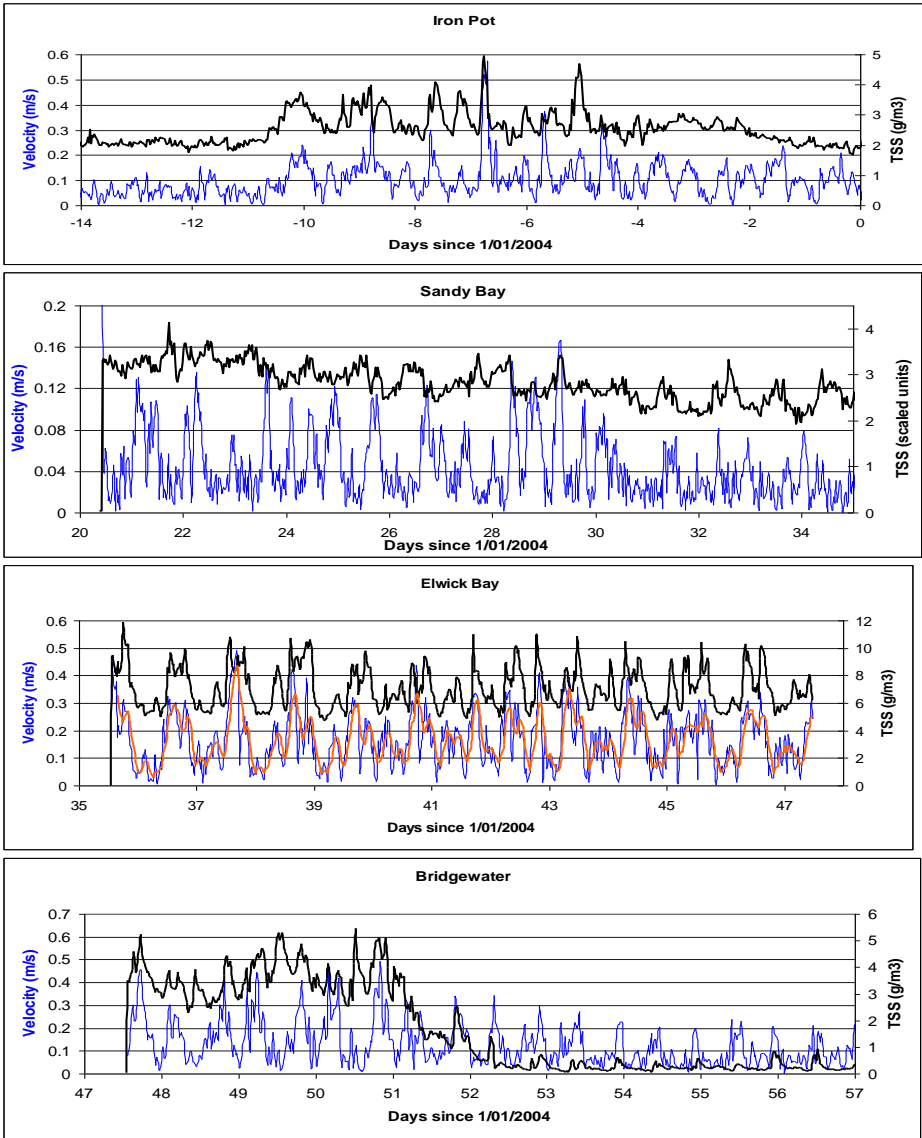


Fig. 7 Measured TSS and currents

Sediment model vs data

The sediment model was calibrated with respect to flocculation parameters (a and b in (11)), settling velocities of unflocculated particles, and critical shear stress of the sediment resuspension. The best fit between model and measurements has been achieved with the flocculation parameters $a=500$, $b=3$; settling velocities for disaggregated silt and clay particles of $2e-4$ and $1e-5$ m/s respectively; and critical shear stress of resuspension of 0.05 N/m².

Figure 7b illustrates comparison between model and data. The model reproduces the low concentration of suspended solids at Sandy Bay site, and the intratidal variability of the sediment concentrations in Elwick Bay. Maximum discrepancies between model and data occur at Bridgewater site and are attributed to the lack of data to specify an accurate initial distribution of sediments in the upper estuary, and to insufficient resolution of the modelling domain in this region.

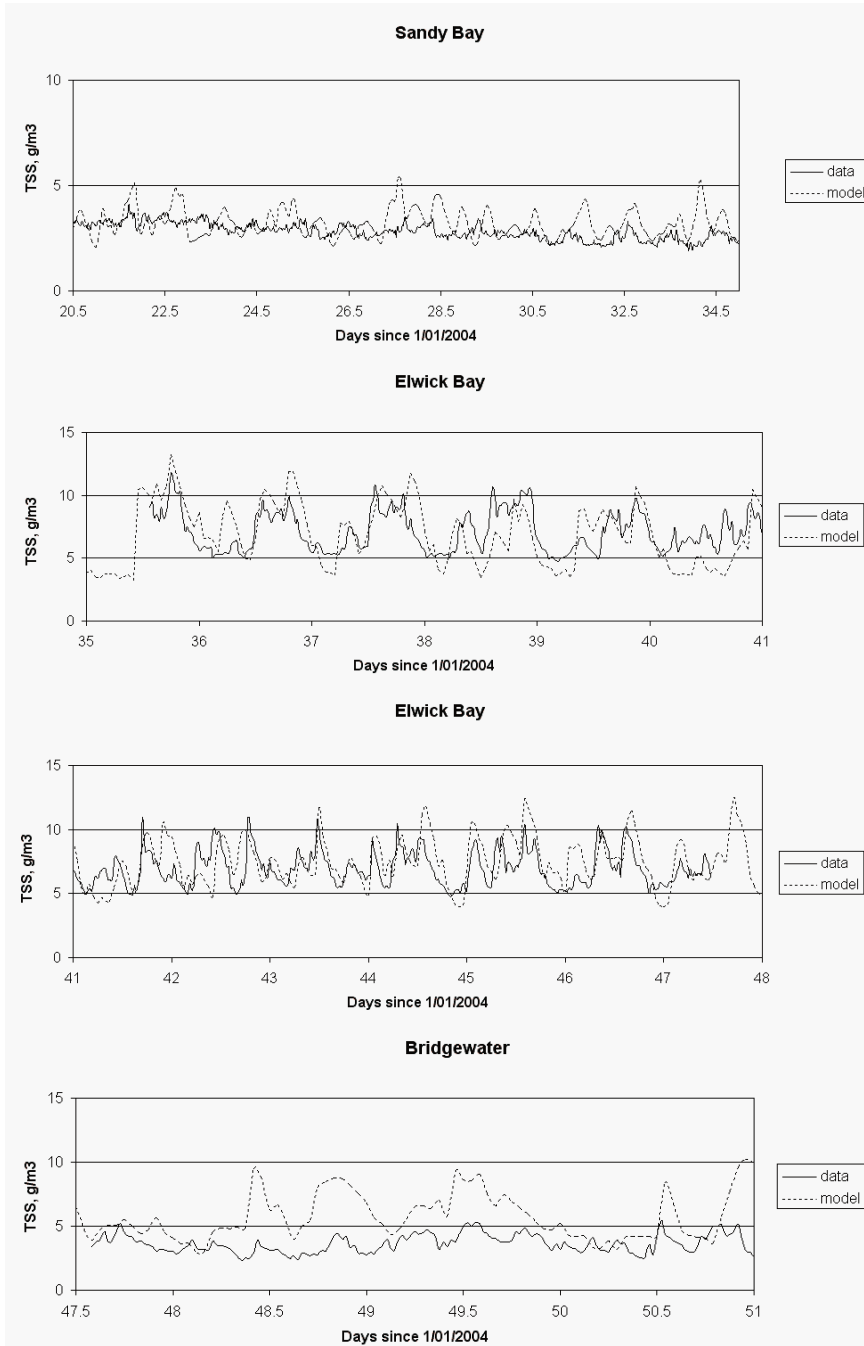


Fig. 7b Measured and simulated suspended sediment concentrations

MODELLING RESULTS

Sediments

Shear stresses and concentrations

According to simulations, during the ebbing and flooding tides the maximum shear velocities tend to develop along the main channel in the northern part of the middle estuary (between Bridgewater and New Town Bay) and in the shallow areas of the lower estuary (fig. 8). In the lower estuary, there is a marked asymmetry of the shear velocity distribution during flooding and ebbing phases of the tide. The flooding tide generates higher friction along the western shore while during the ebb phase of the tide, higher shear velocities tend to develop along the eastern shore. The model predicts elevated shear velocities in the central part of Ralphs Bay and near the southern entrance of the lower estuary, which is characterised by relatively shallow water.

Minimum shear stresses in the lower estuary tend to develop in the middle deep section of the channel, indicating a potential depositional environment. Note that blue colours in figure 8 represent deposition zones (bottom friction less than critical friction for resuspension), yellow and red colours show erosion zones, and green colours represent areas with either zero or relatively weak resuspension or deposition. Bottom friction in the estuarine embayments (such as Sandy Bay, Geilston Bay, New Town Bay, Prince of Wales Bay, Elwick Bay shoals) under moderate and low wind conditions is consistently lower than that in the main channel of the estuary, and lower than the critical shear velocity required for sediment resuspension.

Figure 9 shows time-series of simulated bottom shear velocities at Bridgewater, Elwick Bay, Sandy Bay, and Iron Pot sites. The red line indicates the critical (minimum) shear velocity required for resuspension of fine sediments, and obtained from the model calibration runs. As anticipated, bottom shear velocities are below critical values at Sandy Bay, suggesting a depositional site. On Bridgewater, Elwick Bay and Iron Pot sites, the energy of tidal currents is sufficient for resuspending fine sediments. Under low and moderate river flow conditions, shear velocities at all sites undergo appreciable variability over the diurnal and neap-spring tidal cycle. High friction predicted at Bridgewater site in winter (fig. 9a) is attributed to elevated river-flow events, developed in August and September 2003 (fig. 3).

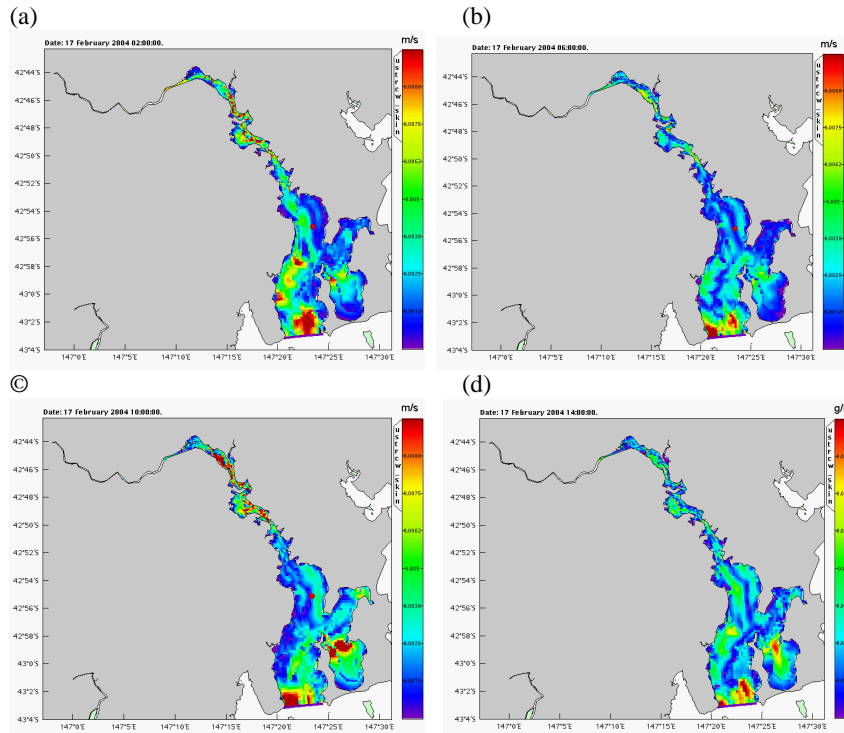


Fig. 8 Shear stresses during spring tide (a) flooding tide (b) high water (c) ebbing tide (d) low water

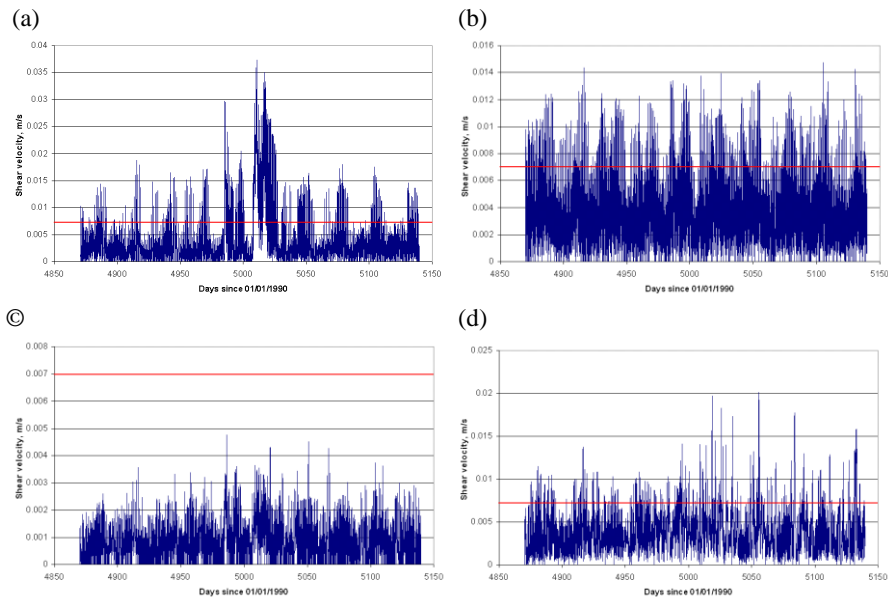


Fig. 9 Shear velocity at (a) Bridgewater, (b) Elwick Bay, and (c) Sandy Bay (d) Iron Pot.

According to the model, under low and moderate river flow conditions, areas of the highest surface concentrations of suspended solids tend to develop between Bridgewater and Elwick Bay (fig. 10a). The model also predicts isolated patches of elevated sediment concentrations in Ralphs Bay. Those patches develop in shallow areas with strong bottom friction, where even small resuspension rates can produce high suspended sediment concentrations because of the small depth of the overlaying water. During elevated discharge events, enhanced resuspension of bottom sediments from the upper and middle estuary develops a plume of concentrated suspension that propagates downstream with fresh water (fig. 10b). Two processes contribute to the development and maintenance of the concentrated suspension during flood events. Firstly, increased bottom friction enhances resuspension of bottom particles and secondly, the increased volume of fresh water represses sediment flocculation, thus decreasing settling velocities of the suspended sediment, allowing turbulent flow to maintain higher concentrations of suspended solids. As the pool of the concentrated suspension propagates downstream, fresh water layer is mixed with the underlying salt wedge, sediments flocculate and settle out of the fresh-water layer with subsequent deposition on the sea-bed.

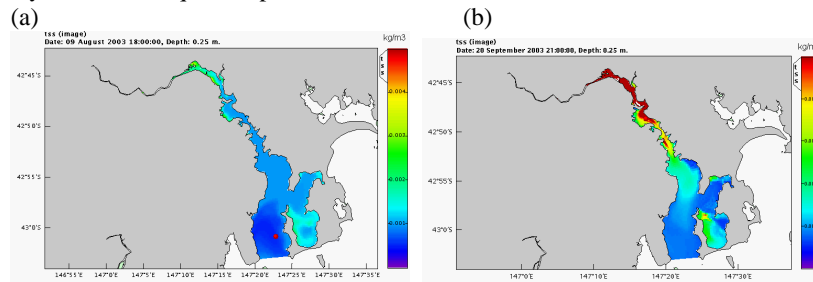


Fig. 10 Simulated surface TSS during (a) moderate ($\sim 80 \text{ m}^3/\text{s}$, high water, spring-tide) and (b) high ($\sim 800 \text{ m}^3/\text{s}$) river-flow conditions.

During high fresh-water discharge events at the Bridgewater site, simulated suspended sediment concentrations near the bottom exceed concentrations near the surface (fig. 11), while at the Elwick Bay site, the suspended sediment concentrations in the surface layer are higher than those near the bottom (fig.12) because of the downstream flushing of sediments. The concentration peak declines as the sediment plume propagates downstream along the estuary, and at the Sandy Bay site, the maximum is close to the background values (fig. 13).

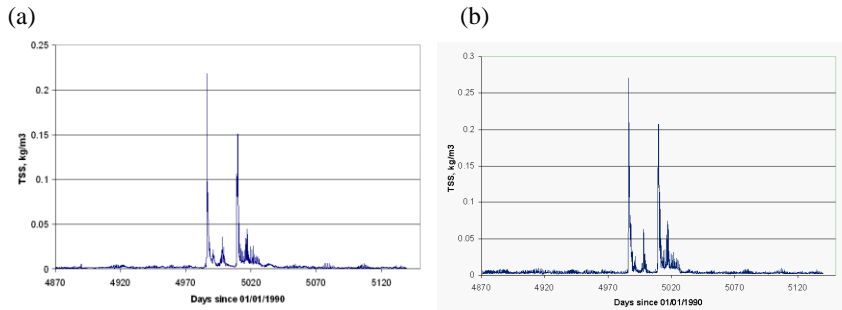


Fig. 11 TSS at Bridgewater (a) surface (b) bottom.

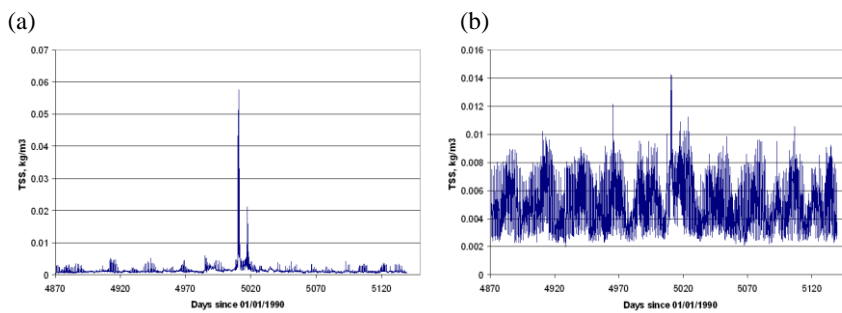


Fig. 12 TSS at Elwick Bay (a) surface (b) bottom

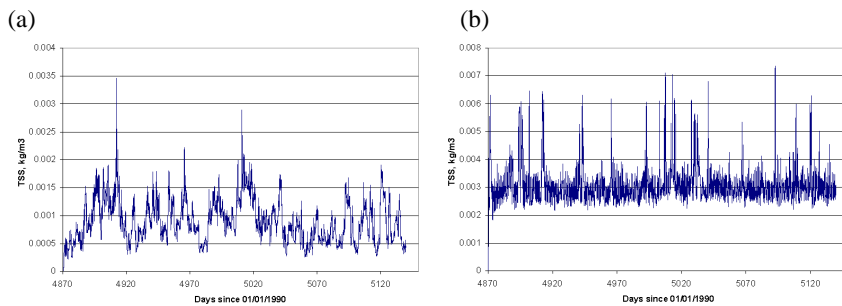


Fig. 13 TSS at Sandy Bay (a) surface (b) bottom

Sediment fluxes

Simulated horizontal fluxes of the suspended sediment show large variability over diurnal and neap-spring tidal cycle (fig. 14). During elevated discharge events, enhanced downstream transport of sediment gradually declines along estuary and vanishes at the estuarine mouth (section 4).

In order to investigate net horizontal fluxes of sediment, instantaneous fluxes, shown in fig. 15, have been integrated over the simulation period and replotted in figure 16. Any point on a particular graph in figure 16 shows the net amount of sediment that has passed through the corresponding estuarine section from the beginning of the simulation up to the given

moment of time. According to the model, net fluxes of the clay fractions of sediment are directed predominantly downstream under all flow conditions. Fluxes of the heavier silt fractions vary with time: under low and moderate flow conditions silt is advected upstream through sections 0-4, while during the high flow events the direction of silt transport changes from upstream to downstream at sections 0-2 (upper and middle estuary). There is little impact of the elevated river discharges on the sediment transport in the lower estuary (section 4), where the net sediment flux is consistently directed upstream. In Ralphs Bay the model predicts net discharge of both silt and clay fractions of sediment to the main body of the estuary.

Figure 17 shows the sediment mass balance over the simulation period for different estuarine boxes. Positive values correspond to sediment accumulation in a box. According to the model, there is net accumulation of sediments in the middle and lower estuary, except areas above Elwick Bay (box 0) and in Ralphs Bay (box 4). Elwick Bay shows the highest rate of the sediment accumulation, which is attributed to episodic depositions during high river-flow events.

A map of simulated thicknesses of the bottom deposits (fig. 18) shows accumulation of sediment in the middle estuary and in the deep central part of the lower estuary that is consistent with the sediment flux data (fig. 17). For the modelled period, the model predicts higher deposition rates in the deep sections of the main channel, and lower rates of the sediment accumulation in shallow embayments (Sandy Bay, New Town Bay, Prince of Wales Bay, Elwick Bay). Note that preferential accumulation of sediments in the deep sections of the estuary might be exacerbated by the step-like representation of the bathymetry in the model.

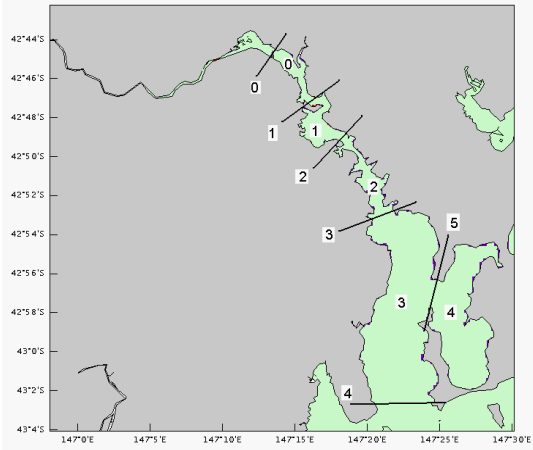


Fig 14. Location map for estuarine cross-sections and boxes

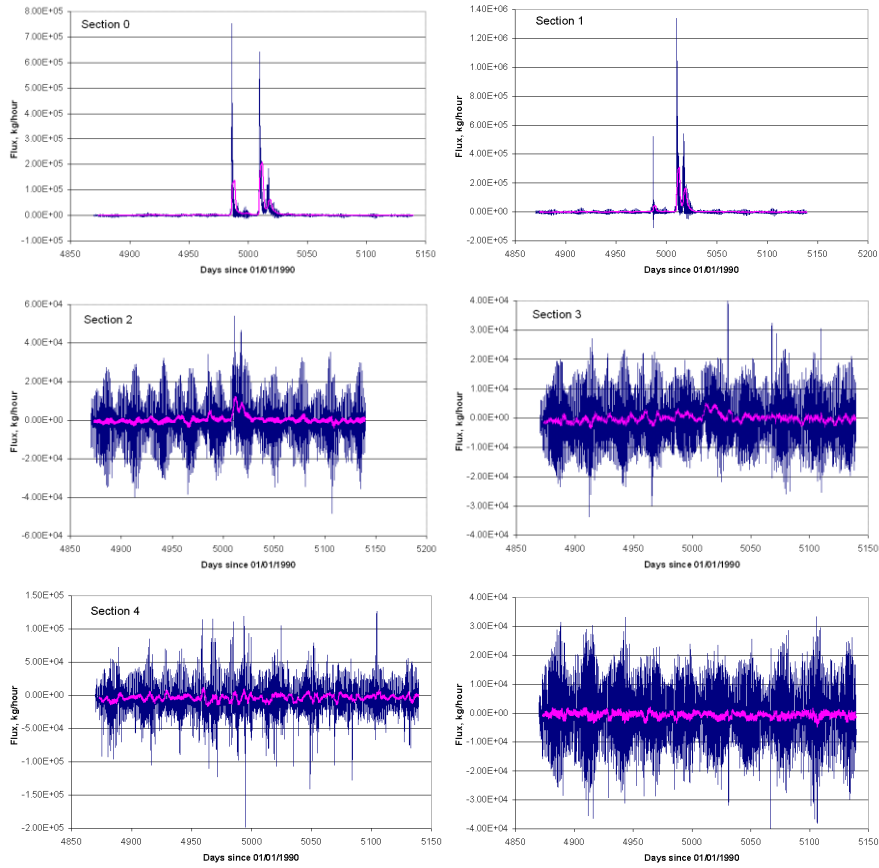


Fig. 15 Instant sediment fluxes (black line), and sediment fluxes with filtered diurnal component (red line). Location map is given in Figure 14. Positive fluxes correspond to downstream direction at sections 0-4 and east-west direction at section 5.

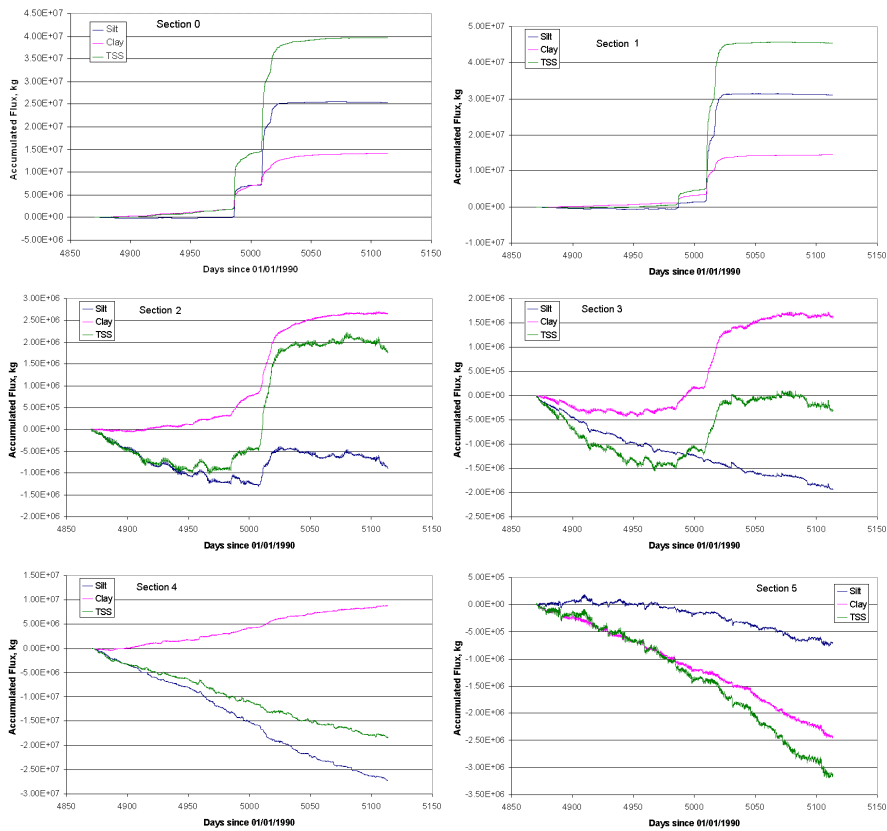


Fig. 16 Accumulated sediment fluxes. Location map is given in Figure 14.

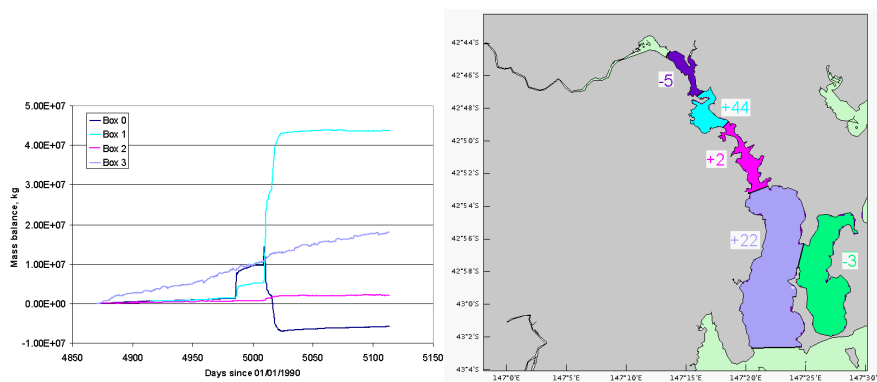


Fig. 17 Sediment mass balance (a) evolution with time (b) net balance, in kT. Location map is given in Figure 14.

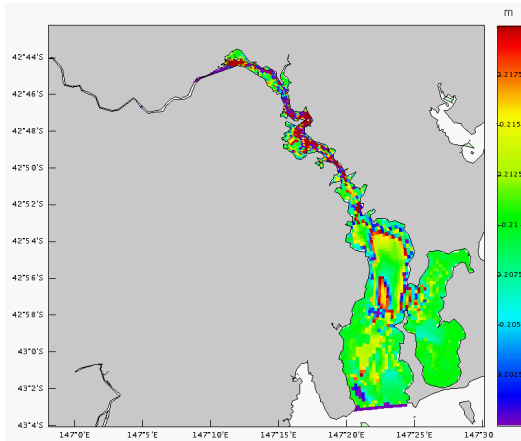


Fig. 18 Sediment thickness after one year modelling

Point sources

Numerical experiments with the sediment-attached tracers, released from point sources, are illustrated in figure 19, which shows distribution of bottom concentrations of the tracers after 9 months modelling. All tracers are released at a constant rate. Most sources are located in the near bottom layers. At the zinc smelter, tracers are released from both near bottom and near surface regions (see source characteristics in table 1). The left and right plots in figure 19 show the same concentration fields but the plots have different concentration scales.

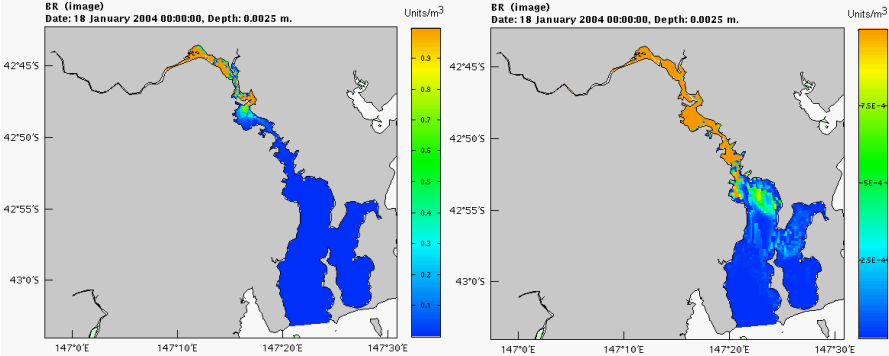
Name	Location	Latitude	Longitude	Depth (m)
BM	Blackmans Bay	-43.016	147.331	5
SB	Blinking Billy at Sandy Bay	-42.915	147.369	17
MP	Macquarie Point	-42.880	147.342	14
RY	Rosny	-42.877	147.359	10
BR	Boyer (Norske Skog)	-42.770	147.103	4.5
PW	Prince of Wales	-42.826	147.304	2
SM_t SM_b	Zinifex smelter	-42.828	147.318	0 (surface) 6 (bottom)

Table 1 : Point source characteristics

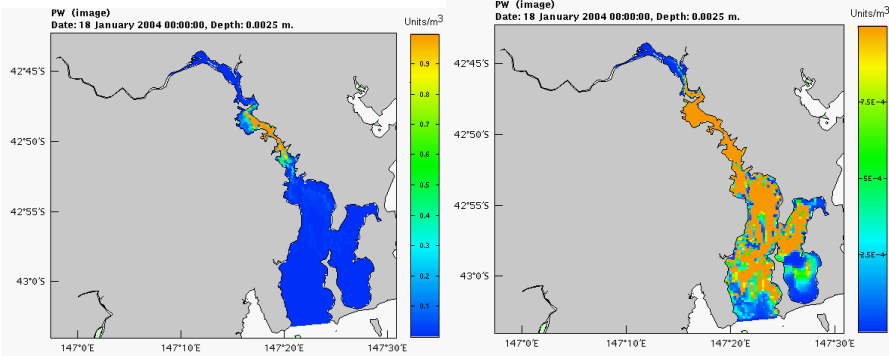
Inspection of the modelling results reveals that under low and moderate flow conditions, tracers released at the Boyer site accumulate in bottom deposits of the upper estuary. During elevated flow events, those deposits are resuspended, transported downstream and redeposited in the middle estuary (fig. 19a). In the middle and lower estuary, regions of the highest concentration of the deposited tracers are located under the release points. Net

upstream propagation of the tracers is mediated by interaction with bottom deposits. After 9 months modelling, concentration of tracers in bottom sediment upstream from Bridgewater does not exceed 0.001 units/m³ for all tracers released in the middle and lower estuary. The concentration of tracers in Ralphs Bay exceeds 0.001 units/m³ only for simulations with the surface release scenario.

Boyer



Prince of Wales



Smelter (bottom release)

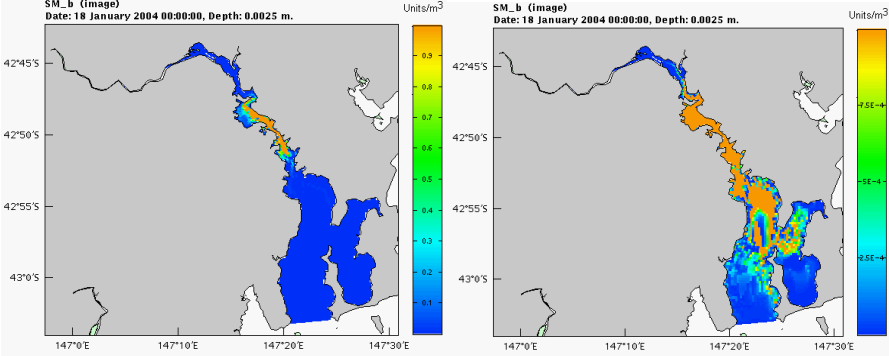
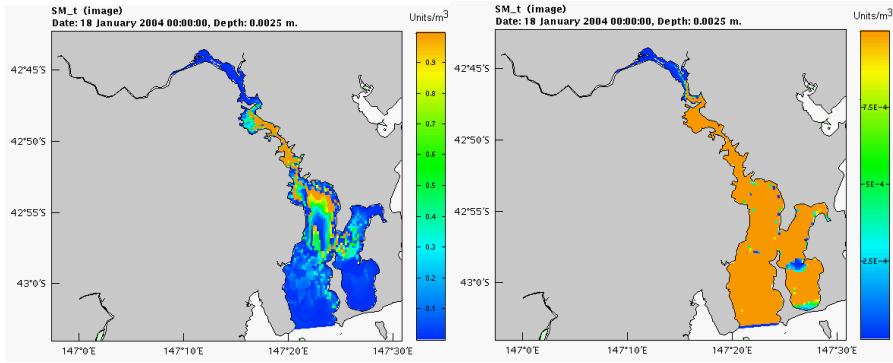
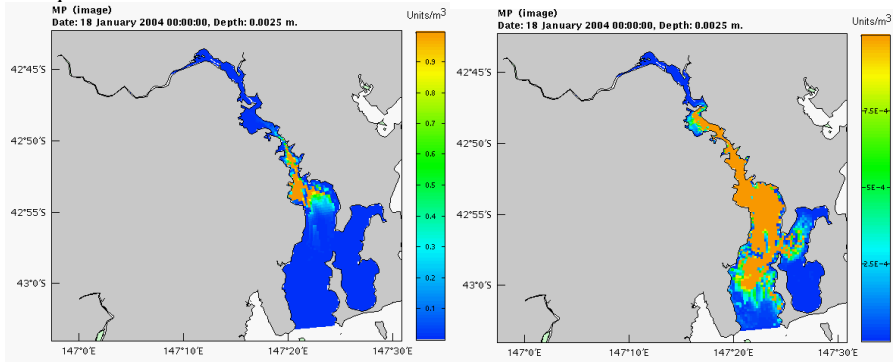


Fig. 19a Bottom concentration of tracers released from point sources.

Smelter (surface release)



Macquarie Point



Rosny

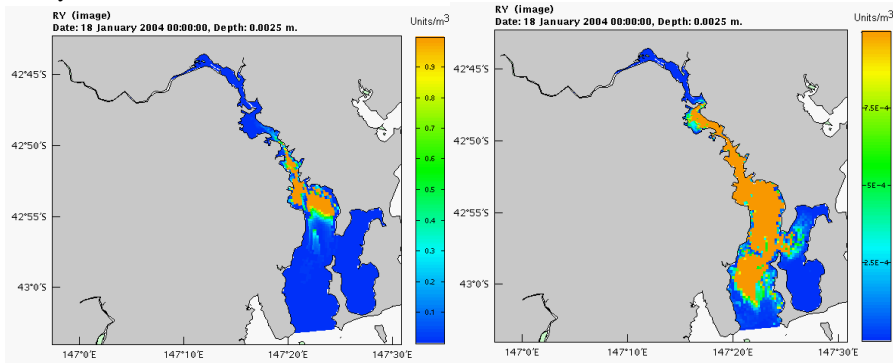
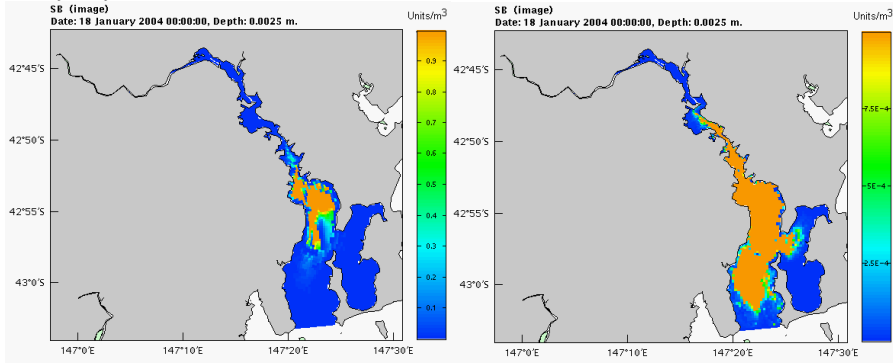


Fig. 19b Bottom concentration of tracers released from point sources.

Sandy Bay



Blackmans Bay

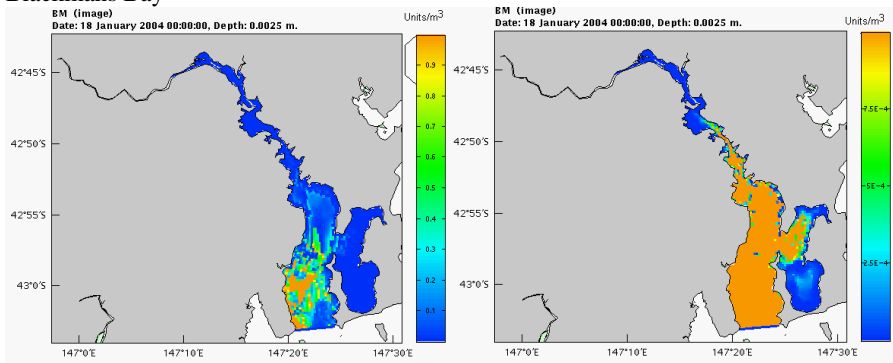


Fig. 19c Bottom concentration of tracers released from point sources.

Zinc

Concentrations

Typical patterns of simulated zinc concentrations at the surface of the estuary are illustrated in figures 20, 21. The distribution of the dissolved zinc correlates with the sea-bed contamination, showing highest concentrations of the metal in the middle estuary, over the areas with the highest level of the sea-bed contamination (fig. 5). The contaminant plume undergoes tidal excursion, with higher concentrations developing in Elwick Bay during high water, and lower concentrations during low water. The particulate zinc in the surface layer does not exceed 10 % of the total concentration, consistent with observations (Green & Coughanowr, 2003).

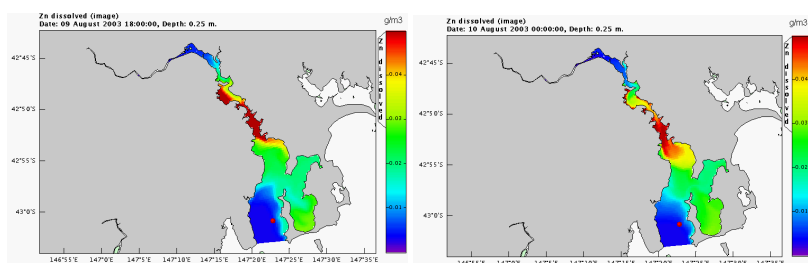


Fig. 20 Surface concentrations of dissolved zinc during (a) high and (b) low water (spring tide)

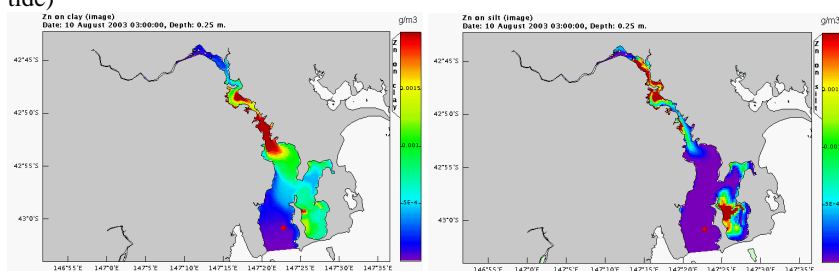


Fig. 21 Surface concentration of zinc attached to sediment
(a) zinc on clay (b) zinc on silt

Numerical modelling suggests that in the middle estuary, which is characterised by a large sedimentary pool of the contaminant (fig. 5), sediments undergo appreciable tidal variability due to periodic resuspension and deposition. When bottom sediments are resuspended, zinc attached to particles, as well as zinc dissolved in pore water, is entrained in overlying water. Zinc from pore water is diluted in surface water. Zinc attached to particles tends to equilibrate with the dissolved zinc. In the water column, which is continuously flushed due to fresh river-flow and baroclinic salt-wage circulation, dissolved contaminants are discharged to the ocean. Hence, the water column is likely to be under-saturated with respect to dissolved contaminants, and some fraction of the metal may be released from suspended particles to water. During the next deposition event sediment particles settle on the bottom, mix with an active sediment layer and adsorb dissolved zinc from the pore water. Adsorbed zinc is released again during the next resuspension event. Cycling of sediment and pore water between sea-bed and water column provides pumping of zinc from contaminated sediments to water column. The concentration of zinc in the

water column establishes as a balance between dissolved contaminant discharge to the ocean and metal supply from sediments; both of those processes are mediated by the sorption and desorption reactions.

A number of numerical experiments have been carried out in order to test the model sensitivity to sorption parameters. According to these runs, increasing the exchange rate from 0.5 to 1 (day^{-1}) increases the concentration of zinc in the water column, while increasing K_d from 20 to $100 \text{ m}^3/\text{kg}$ reduces the concentration of zinc in the water (fig. 22).

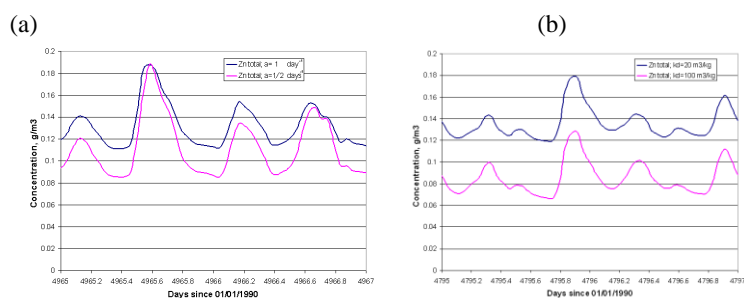


Fig. 22 Concentration of zinc in Elwick Bay, simulated with different sorption parameters (a) $K_d=20 \text{ m}^3/\text{kg}$, $a=1$ or 0.5 day^{-1} ; (b) $K_d=20$ or $100 \text{ m}^3/\text{kg}$, $a=0.5 \text{ day}^{-1}$

Time-series of zinc concentrations at the surface and near bottom layers of Bridgewater, Elwick Bay and Sandy Bay sites (fig. 23-25) show reduced concentrations of the dissolved zinc in surface water during the winter season, due to elevated fresh water discharge. During episodic high flow events, enhanced resuspension of contaminated sediment results in short-term increases of the concentration of particulate zinc at Bridgewater and Elwick Bay sites.

Due to the baroclinic salt wedge circulation, under low and moderate flow conditions, the model predicts higher concentrations of zinc in the bottom layer and lower concentrations in the surface layer at Elwick Bay and Bridgewater sites (upstream from the zinc smelter), and an inverse vertical distribution of zinc at the Sandy Bay site (downstream from zinc smelter). Such vertical distributions of zinc in the estuary agrees with observations, which also show near surface maximum downstream from New Town Bay, and near bottom maximum upstream from Elwick Bay (Green & Coughanowr, 2003, fig. 32).

According to DPIWE Ambient Water Quality data analysis, total zinc levels measured in 2003 surveys have never exceeded 0.1 g/m^3 . Inspection of the data in fig. 23-25 shows that the developed pilot-model likely overestimates concentration of zinc in water. In the near bottom layer of the Elwick Bay site, the modelled concentrations of particulate zinc undergo large tidal variability, with the peak concentrations occasionally exceeding concentrations of the dissolved zinc (fig. 24b). According to observations (DPIWE Ambient Water Quality data analysis), during 2003 surveys concentration of particulate zinc in bottom waters of the Derwent estuary did not exceed 20 % of the total zinc in bottom water.

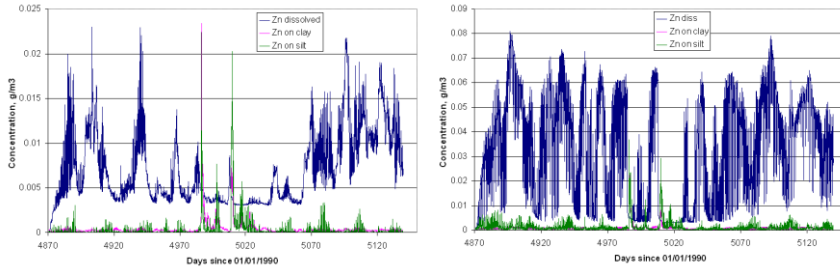


Fig. 23 Zn at Bridgewater (a) surface (b) bottom

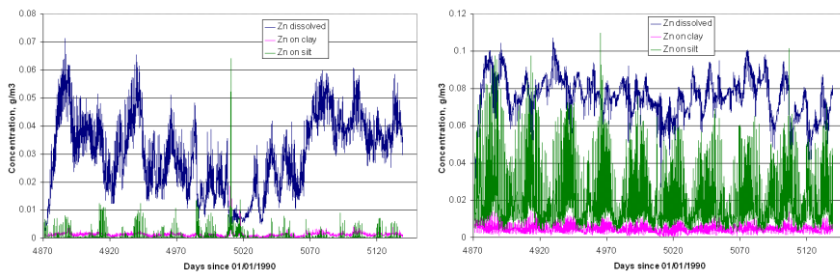


Fig. 24 Zn at Elwick Bay (a) surface (b) bottom a=2 (c) bottom a=1

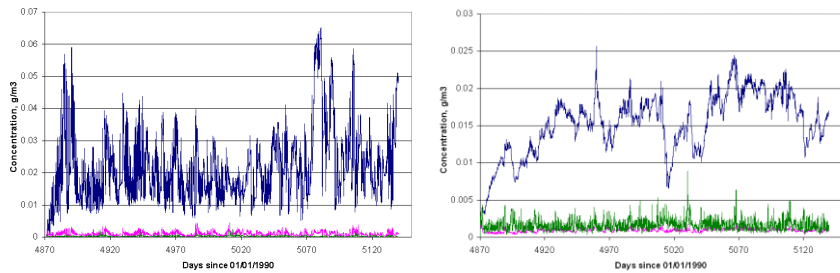


Fig. 25 Zn at Sandy Bay (a) surface (b) bottom

Fluxes

Time-integrated fluxes of zinc (fig. 26) show an elevated flux of zinc out of the upper estuary during high flow events, with a subsequent deposition of contaminated particles and accumulation of zinc in Elwick Bay. At section 2 (between Prince of Wales Bay and Elwick Bay) dissolved zinc is flushed downstream, while particulate zinc is transported upstream, resulting in a net upstream flux of the metal. In the lower estuary (sections 3 and 4) contaminant fluxes are directed downstream. According to the model, for the modelled period, zinc is discharged from Ralphs Bay. The net balance of zinc for estuarine boxes (fig. 27) shows accumulation of zinc in Elwick Bay and net loss of zinc from the upper and lower estuary.

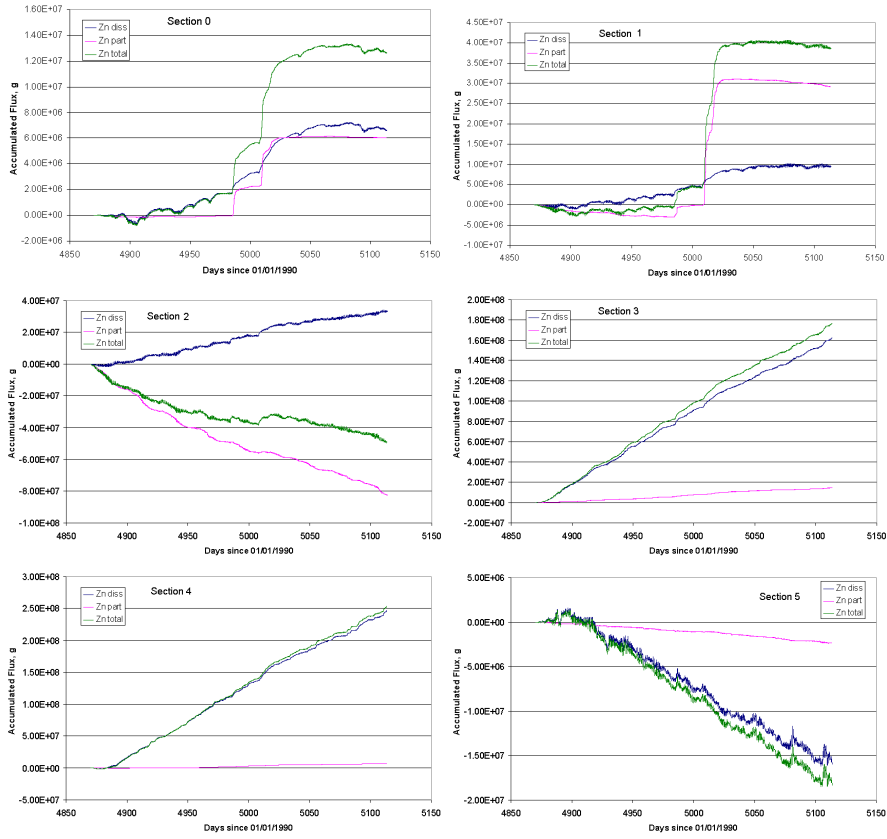


Fig. 26 Accumulated fluxes of zinc

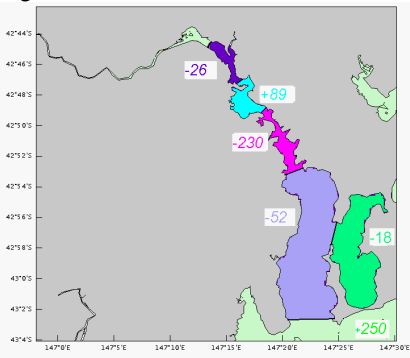


Fig. 27 Mass balance of zinc

Preliminary scenario runs

The modelling described in previous sections was based on an assumption that all zinc attached to sediment is readily available for dissolution and there is no input of zinc from ground water. However limited experimental data (Butler et al., 2005) suggest that most of zinc attached to particles is in a refractory form, and there might be substantial loads of dissolved Zn to the estuary associated with the contaminated ground water input (Green & Coughanowr, 2003).

In this section additional scenarios, involving assumptions on the refractory zinc content and ground water inputs (table 2), are simulated and the modelling results are compared to measurements. According to scenario (A) all particulate zinc is readily available for dissolution and there is no input of dissolved zinc from ground water. In scenario (B) only 25% of initially allocated zinc deposits are available for dissolution from sediments and, again, there is no input of ground water. In scenario (C) all zinc attached to particles is considered as refractory, and hence the only significant source of the dissolved zinc in water column is due to zinc loads associated with the input of the contaminated ground water. Another source of the dissolved Zn in the estuary is associated with the river input, however at the upstream river boundary the concentration of the contaminant (5 mg/ m^3) is much lower than that observed in the middle estuary and, hence, the river input can not explain high levels of zinc in the estuary. Zinc loads from the ground water were represented as near bottom point sources located near Pasmenco, and discharging at a constant rate of 100 t/year (Green & Coughanowr, 2003). Given strong tidal mixing in the estuary and lack of data to specify spatial distribution of the diffusive ground-water sources in more detail, such representation of the external zinc loads, at this stage, seems to be relevant to the model complexity and an accuracy of simulations.

Scenario	Percentage of refractory zinc (%)	Ground water dissolved Zn loads (tonnes/year)	Equilibrium distribution coefficient (m^3/kg)	Sorption/desorption time scale (days)
A	0	0	20	1
B	75	0	20	1
C	100	100	No sorption exchange	No sorption exchange

Table 2 Simulation scenarios

The simulation period is May 2003 – January 2004. The model initially was tested against total zinc concentrations measured at the surface below the Bridgewater causeway during 2000 – 2002 (Green & Coughanowr, 2003). After completion of these tests more data became available for the dissolved and particulate Zn concentrations, measured in the estuary during 2000-2003, and the existing model output was compared to these data as well.

Figures 29-32 show median values of the measured and modelled zinc concentrations; lower and higher error bars show 10 and 90 percentile values respectively. According to these data, predictions based on an assumption of zero content of refractory zinc (scenario A) more than three times overestimate concentrations of total zinc in the middle estuary

(fig. 29). The simulations based on scenario C (100% refractory zinc plus input of the dissolved Zn from ground water) and scenario B (75 % refractory zinc and no ground water loads) produce results surprisingly close to each other and close to measurements (fig. 30-32).

Figure 33 shows concentrations of the dissolved and particulate fractions of zinc as simulated using scenario (C). According to this scenario there is no sorption-desorption reactions and all particulate zinc is permanently attached to particles. The modelling results indicate that only particulate zinc can not explain high levels of the contaminant in the estuary, unless there are additional sources of the dissolved zinc associated with either desorption from particles or/and ground water loads.

Based on this preliminary scenario modelling, it appears that numerical simulations cannot reliably discriminate between scenario with high ground water loads and negligible dissolution from sediment and scenario with the contaminant dissolution from sediments and negligible zinc loads from the ground water. It appears that these scenarios can only be distinguished by experimental studies, which accurately measure the fraction of zinc in bed sediments, which is released when sediments are suspended under field conditions.

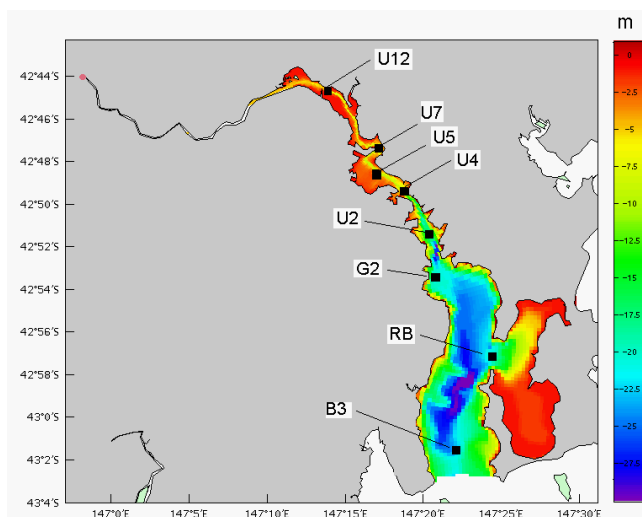


Fig. 28 Water quality monitoring sites

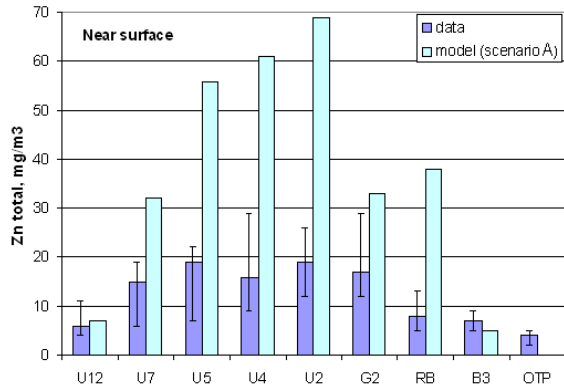


Fig. 29 Modelled concentrations of total Zn (scenario A) vs data. (Location map in fig 28)

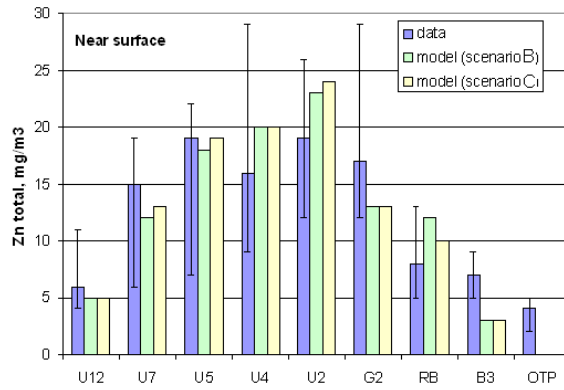


Fig. 30 Modelled concentrations of total Zn (scenarios B and C) vs data. (Location map in fig 28)

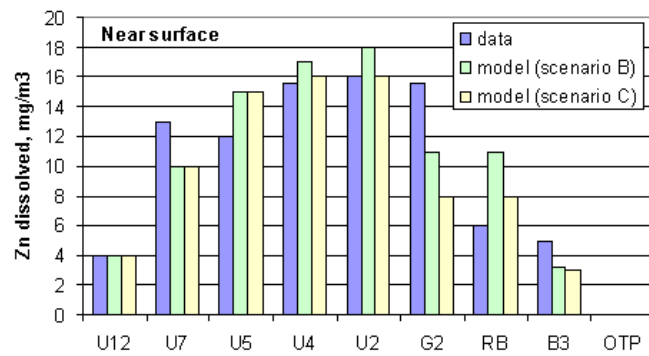


Fig. 31 Modelled concentrations of dissolved Zn (scenarios B and C) vs data. (Location map in fig 28)

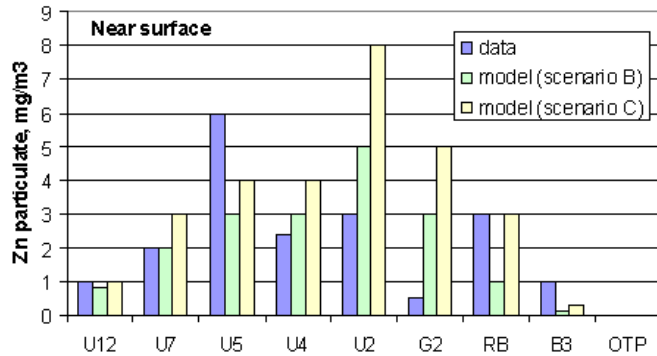


Fig. 32 Modelled concentrations of particulate Zn (scenarios B and C) vs data. (Location map in fig 28)

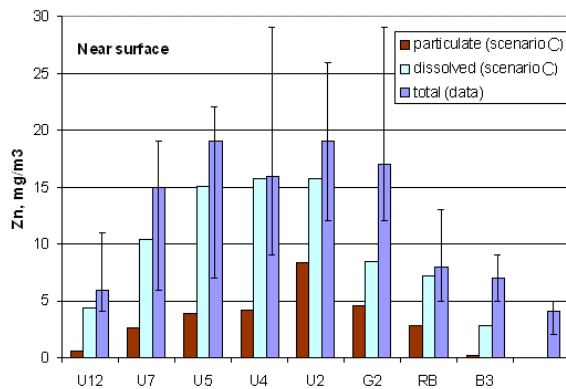


Fig. 33 Modelled concentrations of dissolved and particulate Zn (scenario C) vs total Zn. (Location map in fig 28)

Box-model solutions and implication for management scenarios

In this section a simple box-model of the estuarine zinc transport will be developed and implemented for evaluating the 3-d model predictions and discussing potential implications of the box-model solutions for the management scenarios. For the sake of convenience we start with a brief outline of the problem under consideration. The current external load of dissolved zinc in the estuary is poorly quantified, with a probable range of around 50 to 200 tonnes per year. There is a large and reasonably well quantified pool of zinc in the sediments, but it is not known how much of this is refractory, and how much undergoes exchange with the dissolved phase. The water column concentrations are known quite well from the monthly monitoring program. In the box-model, zinc exchange between the particulate and dissolved phases is represented by a partition coefficient Kd , so that, at equilibrium,

$$\hat{C}_d = \frac{\hat{C}_p}{Kd}, \quad (22)$$

where \hat{C}_d is the dissolved concentration by volume of water (mg/m^3), \hat{C}_p is the particulate soluble concentration by weight of dry sediment (mg/kg), and Kd has units of m^3/kg . The exact value of the parameter Kd is unknown, but literature values range from 2 to 200 m^3/kg . We initially assumed a middle range value of 20 m^3/kg . Note that, if C_p is the sediment concentration of particulate zinc by volume, and we assume a typical density for sediment by volume of $1000 \text{ kg}/\text{m}^3$ (allowing for porosity), then $C_p = 1000 \hat{C}_p$. (In the 3-D model, zinc is assumed to adsorb to clay and silt, but not to sand. In the middle parts of the estuary, the sum of the clay and silt fractions is around $1000 \text{ kg}/\text{m}^3$ (Fig 4). However, at the marine end, the sediments are mostly sand, and the clay and silt fractions fall to values around $200 \text{ kg}/\text{m}^3$ or less. Here, the assumption that $C_p = 1000 \hat{C}_p$ is not valid.)

The 3-D fine-resolution contaminant model described earlier represents the cycling of zinc between dissolved and particulate phases, along with sediment dynamics and hydrodynamics. Unfortunately, the model is computationally expensive, and can be applied to simulate only short periods (one year), and perform a limited number of simulations. We can get some insight into zinc dynamics, and their dependence on these uncertain parameters, by considering a simple two box estuary model, with a sediment layer of thickness Z_s , and volume V_s , and a completely mixed water column of depth Z_w , and volume V_w . If there is no external load, and no flushing, then at steady-state, the concentration C_d in the water column must be at equilibrium with the sediment according to (22). The mass M_w in the water column is just $C_d V_w$, and the mass in the sediment is $C_p V_s$. (We ignore the mass of dissolved zinc in pore water – this is negligible compared with the particulate zinc in the bed. We assume that the water porosity = 1, and concentration by volume of mixture $C_d = \hat{C}_d$. In what follows we also ignore the mass of suspended particulate zinc in the water column – this is small compared with the dissolved pool, but not negligible.). It follows from (22) that:

$$\frac{M_w}{M_s} = \frac{V_w}{V_s(1000 \cdot Kd)} \quad (23).$$

If $Z_w = 10 \text{ m}$ and $Z_s = 10 \text{ cm}$, then $V_w/V_s = 100$, and, assuming $Kd = 20 \text{ m}^3/\text{kg}$, $M_w/M_s = 1/200$. That is, at equilibrium, the mass of available particulate zinc in the estuary sediment is expected to be about 200 times the mass in the water column at any one time.

The observed mass concentrations of particulate zinc in bottom waters in the Derwent range up to around $2000 \text{ mg}/\text{kg}$ in the middle estuary, according to Fig 5. Butler et al (2005) also reported around $2000 \text{ }\mu\text{g}/\text{g}$ (mg/kg) in samples from Elwick Bay. They found maximum pore water concentrations around $50 \text{ mg}/\text{m}^3$ in cores, and observed dissolved concentrations around $30 \text{ mg}/\text{m}^3$ in slurry equilibration experiments. These results suggest values of Kd around 40 to $60 \text{ kg}/\text{m}^3$, if we assume all the particulate zinc is available.

Comment [p1]: I don't understand this sentence, or the distinction between C_d and C_{dhat} .

To this point, we have only considered steady-state relationships, but we can treat dynamics in the two box model, at least in a crude way. We assume there is a load L (tonnes / y), and that the water column is flushed with ocean (or river) water containing zero zinc, with an exchange time T_f . We also assume that the exchange between the zinc in the bed and the dissolved zinc in the water column can be represented by an exchange flux E , which is proportional to $(C_d - C_p / Kd)$.

We can write:

$$E = \frac{(M_w - M_s / (Kd \cdot R))}{T_e} \quad (24)$$

where $R = (V_s / V_w)1000 = 10 \text{ kg} / \text{m}^3$, and T_e is an exchange time constant. There are a number of processes in practice, which can contribute to E , including exchange of pore water with the overlying water column, and adsorption-desorption with resuspended particulate zinc. It is worth noting that doubling the rate constant a for adsorption – desorption changed dissolved concentrations in the 3-D model by about 20% (Fig 22a). This suggests that this rate constant exerts a partial but not controlling influence over the effective exchange rate between water column and bed sediment.

The mass balance of zinc for the water column and sediment gives:

$$\begin{cases} \frac{\partial M_w}{\partial t} = L - \frac{M_w}{T} - (M_w - \frac{M_s}{KdR}) / T_e \\ \frac{\partial M_s}{\partial t} = (M_w - \frac{M_s}{KdR}) / T_e \end{cases} \quad (25)$$

Note that T_e is the effective equilibration time scale for water column dissolved zinc with the bed in the absence of external loads and flushing. A 1-D vertically resolved model, based on the same model formulation as utilised in the 3-d model, suggests this is around 20 days. Note however that the equilibration time scale for the sediment pool is larger than T_e by the factor $Kd * R$. For $Kd = 20 \text{ m}^3/\text{kg}$, $R = 10$, this time scale is around 200 times T_e , or about 4000 days, or 11 years.

Without solving these equations, we can compute approximate concentrations and fluxes for a few limiting situations. If we start loading a clean estuary with dissolved zinc at a constant rate L , the mass concentration in sediments will initially be negligible, and the sediments and flushing will compete as sinks. If we set M_s to be \sim zero, then the water column will quickly approach a state where the load is balanced by losses to flushing and sediments. The quasi-steady state mass in the water column will be given by $M_w = L * T * T_e / (T + T_e)$, and a fraction $T_e / (T + T_e)$ will be exported, with the remainder sequestered in the sediment. Herzfeld et al (2005) give a flushing rate for the Derwent of $T = 11$ days, so we would expect about 2/3 to be exported, but the 3-D contaminant modelling results suggest that the effective flushing time is longer (see below).

After a long enough time, the pool in the sediments is expected to approach chemical equilibrium with the water column concentration. At that point, there will be no net flux to the sediment, and the water column mass will be given by $M_w = L * T$, with the sediment mass given by $M_s = L * T * Kd * R$. Note that the e-folding time scale for equilibration of the sediment with the fixed load is actually given by $Kd * R * (T + T_e)$. For the numbers quoted above, this is around 15 years. Similarly, if the load L was then suddenly reduced to zero, the mass of dissolved zinc in the water column will rapidly approach a quasi-steady state given by $M_w = M_s * T / ((T + T_e) * Kd * R)$, with an export flux of $M_s / ((T + T_e) * Kd * R)$. This concentration and export flux will slowly decay over time, on a time scale of $(T + T_e) * Kd * R$, again around 15 y.

Some of these conclusions can be tested against the scenarios run with the 3-D contaminant model. The 3-D model incorporates spatial and temporal variation at a range of scales, so it is not quite so clear how to compare it with a simple one box model. It would be useful to have a box model which allows some degree of spatial resolution, as an intermediate case. For the moment, we use a rough assumption that V_w is $1.E9 \text{ m}^3$, and $V_s = 1.E7 \text{ m}^3$.

The first scenario run by the model assumed all zinc in the sediment is available, with load $L = 0$. Zinc concentrations in the sediment ranged from around 100 g/kg near the mouth, to over 2000 g/kg in the middle estuary near EZ. Ignoring flushing, we'd expect C_w to range from 5 to 100 mg/ m^3 , and this is quite close to the range predicted by the model. However, allowing for flushing, we'd expect concentrations to be lower by a ratio $T / (T + T_e)$. If the flushing time T were really 11 days, and the exchange time T really 20 days, then model concentrations should be about a third of those ie 1 to 30 mg/ m^3 . However, the effective flushing time for zinc in the model appears to be longer than 11 days. Based on Fig. 20, it looks like the predicted average concentration in the water column is 10 to 20 mg/ m^3 , so $M_w \sim 10 - 20$ tonnes. The calculated annual export is 250 tonnes (Fig. 27), so the effective flushing time appears to be around 0.04 to 0.08 years, or 15 to 30 days. The effective flushing time may be increased because of particle interactions, or the nature and location of the source. Given the strong spatial gradients, it's not a good approximation to treat the estuary as a single well-mixed box.

In the second model scenario, it was assumed that only 25% of the particulate zinc in the sediment is available. The predicted concentrations of dissolved zinc are reduced by a factor of ~3. The simple one-box model also predicts that the water column concentrations should scale linearly with C_p and M_s .

In the third model scenario, the particulate zinc was set to zero, and adsorption turned off, so dissolved zinc effectively acted as a passive tracer. A load of 100 tonnes/y of dissolved zinc was located in the middle estuary. This scenario predicted dissolved concentrations of around 5 to 20 mg / m^3 , which matched observations quite closely. It necessarily exported 100 tonnes/y. Note that total zinc concentrations and export fluxes scaled proportionately in scenarios A & C, suggesting that zinc effectively behaved as a passive tracer in both.

IMPLICATIONS FOR MANAGEMENT SCENARIOS

The management scenarios should take into account the uncertainty in the current loads, and in the percentage of non-refractory particulate zinc in sediments. These uncertainties also interact with uncertainty in the partition coefficient Kd . However, the field observations and experimental results discussed above do impose some important constraints on these parameters. The experimental results of Butler et al (2005) suggest values for Kd around 40 to 60 m³/kg, assuming all the zinc in the sediment is available. We could use smaller values for Kd if we assume a similar reduction in the percent particulate zinc available.

The results for scenario A using the 3-D model show that assuming all bed sediment is available, and setting $Kd = 20$ m³/kg, results in overestimation of observed C_w by a factor of about 2.5, without any groundwater load. This scenario A result seems quite compatible with the slurry experimental results of Butler et al (2005). These also suggested that using $Kd = 20$ m³/kg would result in overestimation of dissolved concentrations by about a factor of 2.5.

One would expect, based on the one-box model, that with zero external load, the predicted water column concentrations would scale with the sediment pool size. We would expect to reproduce the observed concentrations, with zero external load, either by increasing Kd to around 50 m³/kg, or by assuming that only 30% or so of the particulate zinc in sediments is available. In fact, scenario B reproduced observed concentrations of dissolved zinc closely with zero external load under the assumption that 25% of zinc in sediments is available.

Scenario C was run with a load of dissolved zinc of 100 tonnes / y, but zero available zinc in sediment, and no adsorption or desorption. This produced concentrations of dissolved zinc in the water column which closely matched observations. The model necessarily exported 100 tonnes/y, as it had no internal sink.

If we assume that the percent of available zinc in sediments is very low (around 1% or lower), and retain an adsorption / desorption coefficient $Kd = 20$ m³/kg, then the sediment should be a significant sink for zinc. According to the one-box model, if we had run Scenario C with adsorption / desorption switched on, $Kd = 20$ m³/kg, but only 1% of the particulate zinc in sediments available, the predicted dissolved concentrations would have been lower than observed values (or scenario C) by the ratio $T_e / (T + T_e)$. Depending on the effective flushing and exchange times, this ratio might be around 40 to 60%. The same fraction of the load would be exported.

Given the history of zinc loads into the Derwent Estuary, it seems unlikely that the sediments are currently clean or drastically under-saturated with respect to current loads of dissolved zinc. The box model suggests the equilibration timescale for particulate zinc in the sediment under constant load is long, around 15 to 20 y. There is a long history of zinc loads into the Derwent estuary, over many decades, and the last decade has seen large reductions in zinc loads into the estuary. So if anything, we would expect the sediment concentrations of available zinc to be over-saturated compared with current loads; that is, we would expect the sediment to be a net source of dissolved zinc to the water column, not a net sink.

If we accept that the sediment pool should currently be a net source and not a net sink, then we have relatively little room to move, at least for fixed $Kd = 20$ m³/kg. Scenario C shows good agreement between predicted and observed dissolved zinc concentrations, for 25% of

zinc in sediments available, and zero external load. According to the one box model at least, the zinc sediment pool would be in equilibrium with the observed dissolved concentrations in the overlying water column if the % available zinc in sediments was reduced by the ratio $T/(T+T_e)$, to around 15%. That is, with an external load of 100 tonnes / y, and 15% sediment available, we would expect model concentrations to match observed concentrations with zero net exchange between sediment and water column. So the possible combinations of percent availability and external load should lie between these two extremes ie percent available between 15 and 25%, and external load between 100 tonnes/y and zero, with a linear tradeoff.

If we are prepared to vary Kd , we have much more latitude. At any given external load, we effectively have a direct tradeoff between % available particulate zinc and Kd . For zero external load, we could in principle set Kd to 80 m³/kg, and % available to 100, or Kd to 1 m³/kg and % available to 1.25. This does not affect the predicted water column concentrations now, but it does make a huge difference in terms of the size of the available sediment pool, and therefore the timescale for adjustment of this pool to changes in load. Recall that this timescale is given by $(T+T_e) * Kd * R$, and scales directly with Kd . If we reduce % available and Kd from 15% and 20 m³/kg to 0.75% and 1m³/kg respectively, we reduce the sediment pool size by a factor of 20 and the time scale from around 15 years to 0.75 years.

The implications for management are as follows.

If $Kd = 20$ m³/kg and percentage of available zinc is between 15 and 25, then the available sediment pool is large and the adjustment time of this pool to changes in load is several decades. We would expect the sediment is still adjusting to recent reductions in load, and still releasing dissolved zinc. It's likely that the current external load is less than 100 tonnes / y. Reductions in the external load will lead to an immediate reduction in water column concentrations, but not a proportional one, as the efflux from sediments will continue at near current levels for many years.

If $Kd = 1$ m³/kg, and percentage of available zinc = 0.75, then the available sediment pool is small and adjusts rapidly. The sediment is by necessity close to equilibrium with current loads, and net exchange with the water column is close to zero. Reductions in external loads will lead to an almost immediate proportional reduction in water column concentrations.

Note that the observed concentrations of dissolved zinc, combined with the estuarine circulation and mixing, effectively determine an export flux of dissolved zinc from the estuary. It is possible in principle that the exchange of dissolved zinc with suspended sediment could modify this flux, but this appears not to be the case, based on the 3-D model results, comparing scenarios A & C. If this is true, then the current export of zinc from the Derwent is fixed by observations and hydrodynamics at around 100 tonnes / y, independent of any of the uncertain parameters (Kd , percent available).

From a management point of view, the problem can then be summarized as follows. The external load of dissolved zinc into the estuary is almost certainly somewhere between zero and 100 tonnes / y. (It could be more than 100 tonnes / y if the sediment is acting as a net sink, but that seems very unlikely, given the history of loads.)

If the percent of available zinc in sediments is very low, the available sediment pool is small, of similar magnitude to the water column pool of dissolved zinc, and must equilibrate rapidly with current loads. In that case, the current load is around 100 tonnes / y, and we can expect reductions in that load to produce rapid proportional reductions in water column concentrations.

If the percent available zinc in the sediments is large, the pool is also very large, and responds to changes in loads on time scales of decades. Given that external loads have recently decreased substantially, we would expect that efflux from the sediment currently accounts for a significant fraction of the export, and current external loads of dissolved zinc are substantially less than 100 tonnes / y. In that case, it will be difficult to achieve further large reductions in external loads, and these will only be partially translated into reductions in water column concentrations. It will take decades for the efflux from the sediments to decay towards zero.

Scenarios with varying zinc loads from ground water

In the previous sections a number of preliminary model runs have been executed to assess combinations of loads and percentage of available zinc that might be consistent with observations. The modelling included 3-d model runs over annual time-scale and box-model simulations. The box-model simulations covered wide range of temporal scales and provided better understanding of the interactions among K_d , loads, and the percentage of available zinc in determining predicted water column concentrations. In particular, from historical data and box-model solutions it was suggested that the present-day sediments are likely to be over-saturated with respect to zinc and act as a source of the contaminant rather than its sink. This assumption, along with the observed and modelled flushing rates of zinc (100 T/Year), provided additional constraints on the external zinc loads to the estuary limiting them to 0 - 100 T/Year. It was shown also that for a given range of the external loads (0-100 T/Year), and for a fixed $K_d = 20 \text{ m}^3/\text{kg}$, to match model to data, the percentage of the available zinc should lie between 15 and 25%.

The box-model analysis suggests that during short-term simulations, characterised by negligible changes in the sediment pool and quasi-equilibrium state in the water column, scenarios with different K_d and the same ratio of the K_d to the available zinc, predict the same zinc-levels in water column. Hence two unknown parameters K_d and available zinc fraction ($f = C^p_{available} / C^p_{total}$) are reduced into a single parameter: the ratio of K_d to available zinc. For a fixed K_d ($20 \text{ m}^3/\text{kg}$) having known the range of variability of the available zinc fraction (0.15 - 0.25), one can assess the range of this ratio $\frac{K_d}{f} = (80 - 133) \text{ m}^3/\text{kg}$. If this ratio is lower than $80 \text{ m}^3/\text{kg}$ then the rate of dissolution from sediments is high and the model overestimates data, even with zero external loads. If the ratio exceeds $133 \text{ m}^3/\text{kg}$, then the sediments are undersaturated with respect to zinc, and to match model to data, external loads should exceed 100 t/year. Expressing K_d in terms of the total

particulate zinc $\left(\frac{K_d}{f} = \frac{C^p_{total}}{C^d} \right)$, we can assess this ratio from monthly monitoring data.

Figure 34 shows the estimated values of the ratio at a number of sites along the estuary. Note that apart from measurement, these estimates rely also on suspended sediment

concentrations predicted by the sediment model and required to convert volumetric concentrations of the particulate zinc into the mass concentrations. According to these estimates, variations of $\frac{Kd}{f}$ along the Derwent estuary exceed the range of this parameter corresponding to 0-100 T/Year external loads (shown on the plot by red lines). The processes, which control this variability, currently are not understood, and the modelling based on a constant value for $\frac{Kd}{f}$ can not discriminate between scenarios with high and negligible external zinc loads.

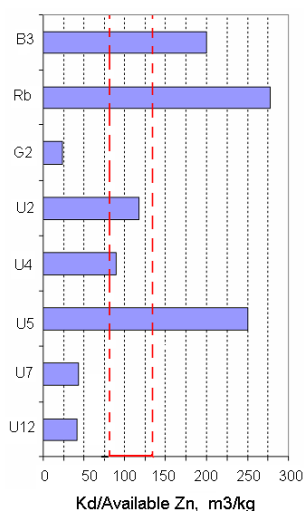


Fig. 34 Estimated ratio of Kd to available zinc fraction at monthly monitoring sites

The model/data analysis, as outlined above, has helped to clarify the constraints on model parameters imposed by observations, and the implications of the remaining uncertainties in those parameters. This understanding has been used to establish a final set of simulation scenarios (Table 3). The main objectives of these scenarios are:

- i) To confirm the simple model analysis, and establish plausible alternative descriptions of the current state (Scenarios D1 and F1).
- ii) To look at the predicted response of the 3-D model to reductions in load (scenarios A1, B1, C1), and incidentally to look at the predicted effect of high historical loads (scenarios E1, G1).

As suggested by the simple model, scenarios with 100T/Year load, and either $Kd = 20 \text{ m}^3/\text{kg}$, and 15% of available zinc (fig. 35a), or $Kd = 1 \text{ m}^3/\text{kg}$, and 0.75% of available zinc (fig. 35b), give equally good agreement with observations. Scaling of Kd and the percentage of the available zinc together resulted in a minor variation of the predicted zinc levels in water column.

The 3-D model predicts a linear relationship between simulated concentrations and loads (fig. 36). This is again consistent with the box-model solutions. From the equation (25), we can derive a steady-state relationship for zinc mass in water column (M_w):

$$M_w = L * T_C + M_s * T_C / (Kd * R * T_e), \quad (26)$$

where $T_C = T * T_e / (T + T_e)$

According to (26) M_w varies linearly with load, with a slope T_C , and an intercept, which represents the effect of the source from the sediment store. Deriving (26) involved an assumption that the sediment pool M_s is fixed. This assumption is violated over long time period when the sedimentary pool equilibrates with the load. However, for $Kd = 20 \text{ m}^3/\text{kg}$ and 15% of available zinc, the sediment equilibration time is long, and over the one year period of the 3-D model run, M_s is close to being constant. Note however that for $Kd = 1 \text{ m}^3/\text{kg}$, and 0.75% of available zinc, the sediment equilibration time is short, and the sediment pool will adjust to the load on a short time scale, considerably less than a year. Under these conditions, zinc mass in water column varies linearly with loads, with a slope T instead of T_C : $M_w = L * T$.

While the box model gives a single linear relationship between zinc concentrations and zinc loads, the 3-d model, which takes into account spatial variability of the flushing rates, predicts a slope of the concentration curves varying along estuary (fig 36).

Figure 37 shows historical data for total zinc concentration in the Derwent estuary. The measurements tend to exceed zinc levels predicted by the 3-d model under scenario E1 (500 T/Year external zinc load), suggesting that zinc loads in 1971 - 1987 have exceeded 500 T/Year. Note however that in scenario E1 the particulate zinc concentrations in sediments reflect current concentrations and availability. The sedimentary pool is in near equilibrium with current loads, and is acting as a sink under the higher loads, thus reducing predicted water column concentrations of zinc. A box model analysis suggests significant variations of the water column concentrations due to such non-equilibrium initial settings. However, additional 3-d simulations carried out under scenario with a low impact of the sedimentary pool on the dissolved concentrations (scenario G1) show only a minor increase of the contaminant levels in water column (fig. 37). The discrepancies between box model solution and 3-d model predictions are attributed to high spatial variability of the zinc cycling processes in the estuary not captured by the box model.

Comment [p2]: This should not be true for scenario G1. You should show G1 conc in Fig 36 as well.

Scenario	Zinc loads (T/Year)	Zn available (%)	Kd (m^3/kg)
A1	0	15	20
B1	25	15	20
C1	50	15	20
D1	100	15	20
E1	500	15	20
F1	100	0.75	1
G1	500	0.75	1

Table 3 Scenarios with varying ground water zinc loads.

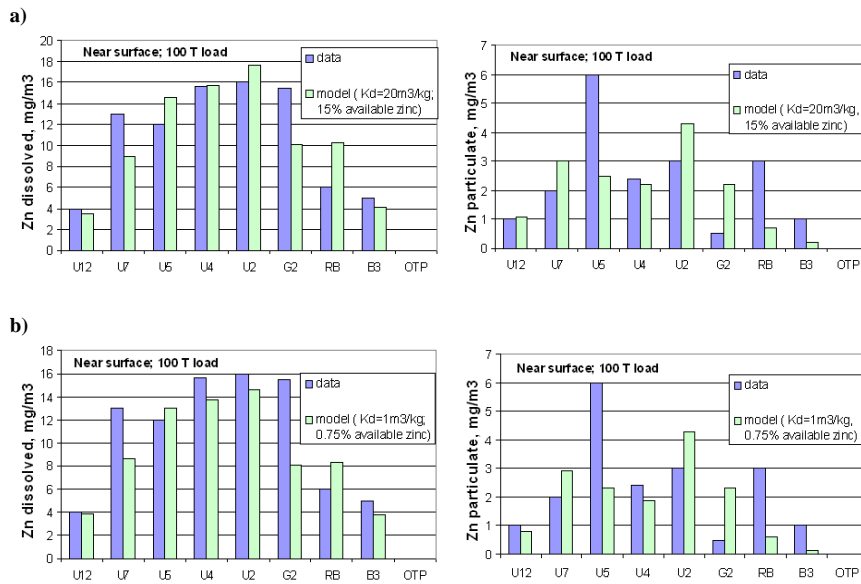
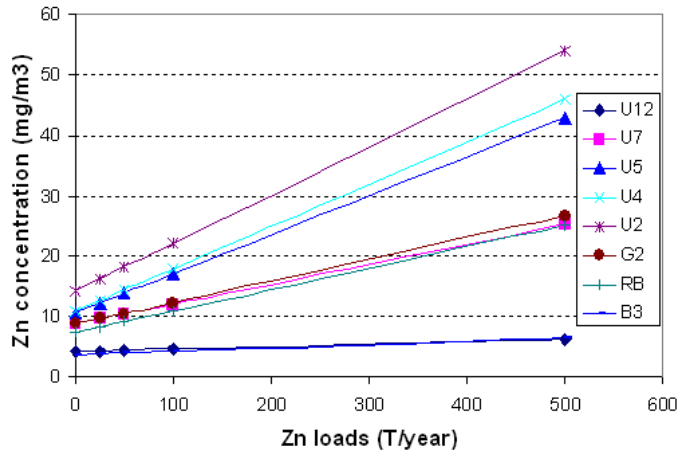


Fig. 35 Modelled concentrations of zinc vs data.

a)



b)

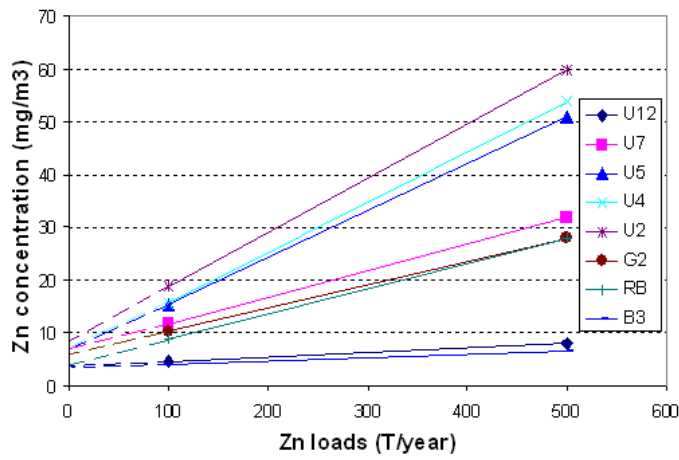


Fig. 36 Concentration of total zinc at different sites as a function of the ground water zinc loads (A) $Kd=20 \text{ m}^3/\text{kg}$, 15% of available particulate zinc; (B) $Kd=1 \text{ m}^3/\text{kg}$, 0.75% of available particulate zinc.

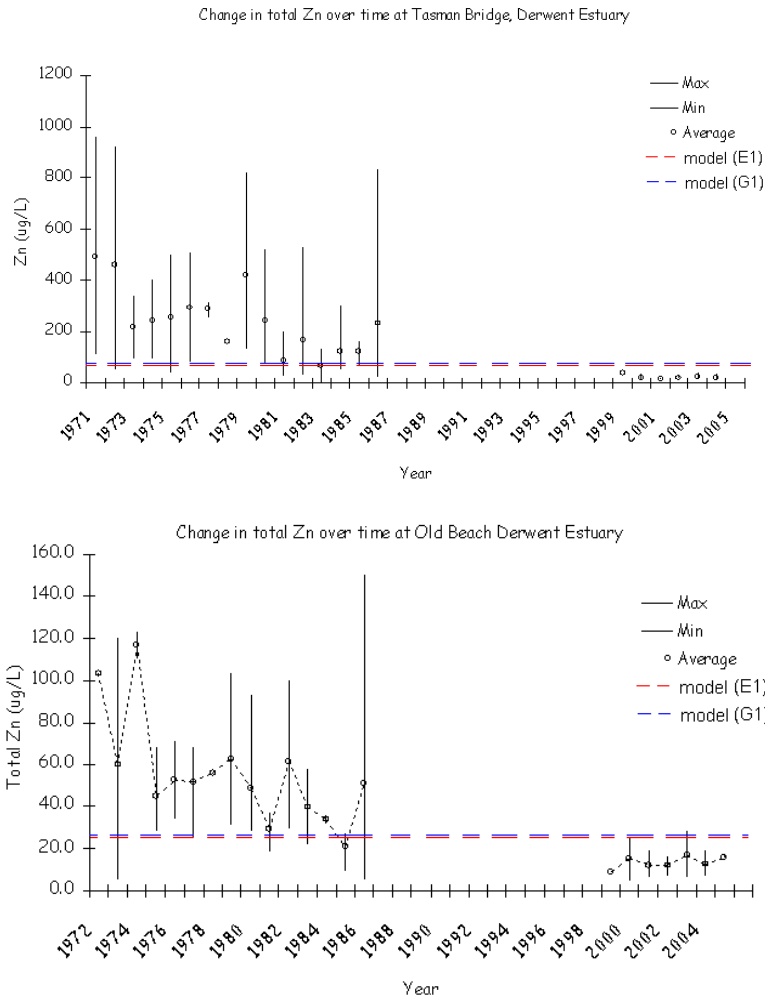


Fig. 37 Historical data on zinc concentrations in the Derwent estuary vs modelled concentrations according to scenarios with 500 T/Year zinc load (scenarios E1, G1)

CONCLUSION

A 3-dimensional fine-resolution numerical model was developed and applied to simulate fine sediment and zinc transport in the Derwent estuary. The model is fully coupled to a 3-dimensional non-stationary, non-linear hydrodynamic model and solves advection-diffusion equations for the mass conservation of zinc and sediments taking into account bottom exchanges due to resuspension and deposition. It represents zinc as dissolved and sediment attached fractions, and employs first order kinetic reaction approach to simulate the contaminant cycling between the solid and liquid phases.

The sediment model was initialised with sediment survey data mapping the distribution of sand, silt and clay fractions of sediment, and calibrated against measured suspended sediment concentrations. The calibrated model was applied to simulate fine sediment transport under varying river flow regimes. Under low and moderate flow conditions ($Q < 150 \text{ m}^3/\text{s}$), the model predicts a net upstream flux of fine sediment in the Derwent estuary due to tidal resuspension and baroclinic (salt-wedge) circulation. During high discharge events ($Q > 500 \text{ m}^3/\text{s}$), enhanced resuspension of bottom sediments in the upper and middle estuary develops a plume of concentrated suspension that propagates downstream with fresh water. As this plume and its associated freshwater layer mix with the underlying salt wedge, sediments flocculate out and settle out onto the sea bed. For the period modelled (May 2003 to Jan 2004), the model predicts a net discharge of fine sediment from the upper estuary and from Ralphs Bay and accumulation of particles in the middle and lower estuary. The highest sedimentation rate, predicted in Elwick Bay, is attributed to episodic redistribution of bottom sediments during high flow events in August and September 2003 ($Q_{\text{max}} \sim 700 \text{ m}^3/\text{s}$ and $900 \text{ m}^3/\text{s}$, respectively).

The zinc transport model was initialised with the observed zinc distribution in bottom sediments. Pilot model runs were conducted assuming zero external zinc loads from ground water and other sources, and using literature data for sorption/desorption parameters. In these simulations, zinc was supplied to the water column through efflux from sediments, and the predicted distribution of zinc in surface water under low and moderate flow regimes correlated broadly with the prescribed zinc concentrations in the sea-bed, with highest surface concentrations of zinc developed in the middle estuary between Elwick Bay and the Tasman Bridge – consistent with observations.

The Derwent Estuary is a stratified, salt wedge estuary, with mean flow directed upstream in bottom waters and downstream in surface waters. As a result of this estuarine circulation, combined with tidal mixing, zinc gradually spreads along the estuary out of the area of highest contamination, with the net fluxes directed upstream above Elwick Bay and downstream below Tasman Bridge. During flood events, the contaminant maximum in the water column is flushed downstream and diluted in the lower estuary. While the concentration of the dissolved zinc drops during runoff events, total zinc levels increase sharply, due to enhanced resuspension of zinc attached to sediments. Thus, particulate zinc, along with bottom sediments, are transported from the upper estuary downstream to the middle and lower estuary during flood events. So one can think of the distribution of zinc in bottom sediments as being controlled by a balance between low to moderate flow periods, during which some zinc is slowly transported upstream by the estuarine circulation, and high flow events during which sediments and attached zinc are transported downstream. For the flow regime from May 2003 to January 2004, the predicted net balance of zinc in

the estuary shows accumulation of the contaminant in Elwick Bay and net loss of zinc from the remainder of the estuary, particularly the middle estuary.

A preliminary attempt was made at calibration of the pilot model. Model calibration was designed to address three major areas of uncertainty.

- The current external loads of zinc to the estuary are uncertain. They are thought to be dominated by loads from groundwater in the vicinity of the Zinifex Hobart Smelter, and total loads are thought to be of the order of 100 tonnes p.a. (Green & Coughanowr, 2003).
- The equilibrium constant controlling the partitioning of Zn between the dissolved and particulate phase, K_d , is uncertain. Literature values for K_d range from 2 to 200 $\text{m}^3 \text{kg}^{-1}$. An intermediate value of 20 $\text{m}^3 \text{kg}^{-1}$ was assumed in the preliminary runs.
- It is thought that a substantial fraction of the Zn attached to bed sediments may be inert or highly refractory, and unavailable for exchange with pore waters or the overlying water column. We have measurements of total zinc in bed sediments, but do not know what proportion of this is available for dissolution.

A series of model runs were conducted to examine the ability of the model to reproduce observed distributions of dissolved and particulate zinc in the estuary water column under different assumptions about these parameters. The key conclusions were as follows:

1. The model alone is not able to discriminate between external loads, and efflux from bed sediments. The model produced equally good agreement between predicted and observed concentrations of dissolved zinc in the water column for two scenarios. The first assumed an external load of dissolved zinc of 100 tonnes p.a., and no exchange of zinc with sediments (ie no zinc efflux from bottom sediments). The second assumed no external load, and around 25% of available zinc in sediments.
2. It is possible to assert with a fair degree of confidence that the estuary currently exports around 100 tonnes dissolved zinc p.a. That is, any model having the predicted circulation (which agrees well with observations), and reproducing the observed water column zinc concentrations, will export around 100 tonnes Zn p.a. Thus, we can be fairly confident that the combined net load of Zn into the water column, from both external sources and bottom sediments, was around 100 tonnes Zn p.a. during the study period.
3. The observations, and some process studies carried out on sediment samples (Butler et al., 2005) help to constrain the ratio of K_d to the fraction of available Zn in bed sediments, but do not constrain either parameter separately, since the measured dissolved concentrations were in equilibrium with sediments. Additional experiments are required to establish Zn sorption curves for Derwent sediments.

Following these attempts at model calibration, two remaining areas of uncertainty have been considered and implications to management were discussed. First, while the total input of dissolved zinc to the Derwent water column is thought to be around 100 tonnes p.a., the modelling alone is not able to determine the relative contributions of external loads and sediment efflux. However, it should be noted that, if the estimates of external loads in (Green & Coughanowr, 2003) turn out to be accurate, then the external load from groundwater and other sources contributes most or all of the 100 tonnes p.a. Second, it is possible that K_d and % available zinc in bed sediments are both high (say 20 $\text{m}^3 \text{kg}^{-1}$ and 15%), or both low (say 1 $\text{m}^3 \text{kg}^{-1}$ and 0.75%).

In a long-term perspective, considering the response of the estuary to the changes in Zn loads over decades, these areas of uncertainty are related. If the % available zinc is less than 1%, then the pool of available zinc in bottom sediments is also low. In this case, simple box models suggest that this pool will respond to changes in external loads of available Zn on short-time scales of around 1 year. If the % available Zn in bottom sediments is high, the pool is large, and will respond to changes in external loads on time scales of decades.

Annual Zn loads from the Zinifex smelter have declined by almost an order of magnitude over the last two decades. If the pool of available Zn in bottom sediments responds slowly, on time scales of decades, one would expect it to be still adjusting to this reduction of external loads, and would therefore expect a significant efflux of dissolved Zn from bottom sediments to the water column. If the pool responds quickly, on time scales of a year, then it would be roughly in equilibrium with current loads, and in this case the net efflux from bottom sediments would be small.

The response time scale of bed sediments also has important implications for the time scale on which reductions in external loads would result in decreases in water column concentrations of dissolved Zn. If the response time is short, water column concentrations are driven primarily by current external loads, and reductions in external loads would result in proportionate and rapid reductions in water column concentrations, on time scales of a year. One could think of this as a rapid-response management scenario. If the response time is long, water column concentrations are driven substantially by efflux from bottom sediments. Reductions in external loads will lead to a partial reduction in water column concentrations in the short-term, but it will take many years to see the full response. We can think of this as a slow-response management scenario. Finally, it's worth noting again that these two scenarios might be distinguished by appropriate Zn sorption experiments conducted with bottom sediments.

REFERENCES

1. Ambrose R.B., Wool T.A., Martin J.L. (1993) The water quality analysis simulation program, WASP5 Part A: Model Documentation. Environmental Research Laboratory, Athens, Georgia 30613.
2. Ariathurai R., Krone R. B. (1976) Finite element model for cohesive sediment transport. *J. Hydraul. Div. ASCE*, 104, HY2, 323-328.
3. Butler E., Leeming R., Watson R., Armand S., Green M. (2005) Final Report on Sediment Resuspension Experiment for Derwent CCI Project
4. Dayer K.R. 1989. "Sediment processes in estuaries: future research requirements". *J. Geophys. Res.*, 94(C10), 14327-14339.
5. Delo E.A. 1988. Estuarine muds manual. Tech. Rep. SR164, Hydraulic Res., Wallingford, England.
6. Green G., Coughanowr C. 2003. State of the Derwent estuary 2003: a review of pollution sources, loads and environmental quality data from 1997-2003. Derwent estuary Program, DPIWE, Tasmania.
7. Fisher F., Simmons V. (1977) Sound adsorption in sea water. *J. of Acoustic Society of America* 62 (3), p. 558-564.
8. Hansen A., Leckie J. (1998) Time-dependent adsorption in near coastal marine sediments: a two-step model. *Advances in water resources* 21, 523-531
9. Hatje V., Payne T., Hill D., McOPrist G., Birch G., Szumczak R. (2003) Kinetics of trace element uptake and release by particles in estuarine waters: effect of pH, salinity and particle loading. *Environment International*, 29, 619-629
10. Herzfeld M., Parslow J., Margvelashvili N., Andrewartha J.R. and Sakov P. (2005) Numerical Hydrodynamic Modelling of the Derwent Estuary. CMR Final Report.
11. Herzfeld M, Waring J., Parslow J., Margvelashvili N., Sakov P. and Andrewartha J. (2002) MECO: Model for Estuaries and Coastal Oceans, scientific manual. CSIRO Marine Research.
12. Holdaway G., Thorne P., Flatt D., Jones S., Prandle D. (1999) Comparison between ADCP and transmissometer measurements of suspended sediment concentration. *Continental Shelf Research* 19, p. 421-441.
13. Jones B., Chenhall B., Debretson F., Hutton A. (2003) Geochemical comparisons between estuaries with non-industrialised and industrialised catchments: the Huon and Derwent river estuaries, Tasmania. *Australian Journal of Earth Sciences*, 50, 653-667.
14. Millward G., Liu Y. (2003) Modelling metal desorption kinetics in estuaries. *The science of the total environment*. 314-316, 613-623.
15. Onishi Y., Dummuller D.C., Trent D.S. (1989) Preliminary Testing of Turbulence and Radionuclide Transport Modeling in Deep Ocean Environment. PNL-6853, Pacific Northwest Laboratory, Richland, Washington.
16. Onishi Y., Serne J., Arnold E., Cowan C., Thompson F. (1981) Critical review: radionuclide transport, sediment transport, water quality, mathematical modelling and radionuclide adsorption/desorption mechanism. NUREG/CR-1322, Pacific Northwest Laboratory, Richland, 512 pp.
17. Plaschke R., Dal Point G., Butler E. (1997) Mercury in the waters of the Derwent Estuary – Sample treatment and analysis. *Marine Pollution Bulletin*, v. 34, N 3, pp 175-185.
18. Turner A., Millward G. (2002) Suspended particles: their role in estuarine biogeochemical cycles. *Estuarine, Coastal, and Shelf Science*, 55, 857-853.

19. Thorne P., Hardcastle P., Soulsby R. (1993) Analysis of Acoustic Measurements of Suspended Sediments. *J. of Geophysical Res.*, V. 98. No. C1, p. 899-910.
20. Thorne P., Hanes D. A review of acoustic measurements of small-scale sediment processes. (2002) *Continental Shelf Research* 22, p. 603-632.
21. Uncles R.J., Stephens J.A. 1989: Distribution of suspended sediment at high water in a macrotidal estuary. *J. Geophys. Res.*, 94(C10), 14395-14405.
22. Walker S.J., Sherwood C.R. A transport model of Port Phillip Bay. CSIRO, Division of Oceanography, Technical Report N 39, 1997, p.59.
23. Wim van Leussen (1999) The variability of settling velocities of suspended fine-grained sediment in Ems Estuary. *Journal of Sea Research*, 41, p. 109-118.
24. Zheleznyak M., Demchenko R., Khursin S., Kuzmenko Yu., Tklich P., Votuk N. (1992) Mathematical modelling of radionuclide dispersion in the Pripyat-Dnieper aquatic system after the Chernobyl accident. *The Science of Total Environment*, 112, 89-14 pp.

APPENDIX 1: Box-model solution

The box-model equations (25),

$$\begin{cases} \frac{\partial M_w}{\partial t} = L - \frac{M_w}{T} - (M_w - \frac{M_s}{KdR})/Te \\ \frac{\partial M_s}{\partial t} = (M_w - \frac{M_s}{KdR})/Te \end{cases}$$

enable exact solution, which can be written as

$$M_w = \frac{B_1}{Kd \cdot R \cdot Te \left(\gamma_1 + \frac{1}{T} + \frac{1}{Te} \right)} \exp(\gamma_1 t) + \frac{B_2}{Kd \cdot R \cdot Te \left(\gamma_2 + \frac{1}{T} + \frac{1}{Te} \right)} \exp(\gamma_2 t) + L \cdot T ;$$

$$M_s = B_1 \exp(\gamma_1 t) + B_2 \exp(\gamma_2 t) + L \cdot Kd \cdot R \cdot T ;$$

where

$$\gamma_{1/2} = \frac{-1}{2} \left(\frac{1}{Kd \cdot R \cdot Te} + \frac{1}{T} + \frac{1}{Te} \right) \pm \sqrt{\frac{1}{4} \left(\frac{1}{Kd \cdot R \cdot Te} + \frac{1}{T} + \frac{1}{Te} \right)^2 - \frac{1}{T \cdot Te \cdot Kd \cdot R}}$$

and B1, B2 constants are to be found from initial conditions

$$M_w|_{t=0} = \frac{B_1}{Kd \cdot R \cdot Te \left(\gamma_1 + \frac{1}{T} + \frac{1}{Te} \right)} + \frac{B_2}{Kd \cdot R \cdot Te \left(\gamma_2 + \frac{1}{T} + \frac{1}{Te} \right)} + L \cdot T$$

$$M_s|_{t=0} = B_1 + B_2 + L \cdot Kd \cdot R \cdot T$$

$$R = \left(\frac{V_s}{V_w} \right) \cdot (\text{Conc of sed in seabed})$$